

**STRUCTURE AND TRANSPORT IN TRIALKYLTRIAZOLIUM IONIC LIQUIDS: A
COMBINED PFG-NMR DIFFUSION AND CONDUCTIVITY STUDY**

by

Sage R. Bowser

B.S. Chemistry, Carnegie Mellon University, 2007

Submitted to the Graduate Faculty of the

Kenneth P. Dietrich School of

Arts and Sciences in partial fulfillment

of the requirements for the degree of

Master of Science

University of Pittsburgh

2013

UNIVERSITY OF PITTSBURGH
DIETRICH SCHOOL OF ARTS AND SCIENCES

This thesis was presented

by

Sage R. Bowser

It was defended on

August 30, 2013

and approved by

Dr. Dennis Curran, Professor, Department of Chemistry

Dr. Sunil Saxena, Professor, Department of Chemistry

Dr. Stephen Weber, Professor, Department of Chemistry

Dr. Damodaran Krishnan Achary, Associate Research Professor, Department of Chemistry

**STRUCTURE AND TRANSPORT IN TRIALKYLTRIAZOLIUM IONIC LIQUIDS: A
COMBINED PFG-NMR DIFFUSION AND CONDUCTIVITY STUDY**

Sage R. Bowser, M.S.

University of Pittsburgh, 2013

Copyright © by Sage R. Bowser

2013

**STRUCTURE AND TRANSPORT IN TRIALKYLTRIAZOLIUM IONIC LIQUIDS: A
COMBINED PFG-NMR DIFFUSION AND CONDUCTIVITY STUDY**

Sage R. Bowser, M.S.

University of Pittsburgh, 2013

ABSTRACT

Ionic liquids (ILs), the class of salts with melting points below 100 °C, are promising alternatives to molecular solvents. Their great chemical tuneability opens the possibility of tailoring ILs for specific tasks; however, data from systematic structure-property studies of ILs, as well as a more complete understanding of the liquid structure and interionic interactions within ILs, are required for the rational design of ILs.

In this thesis, a systematic study of the effect of alkyl chain length and alkyl chain branching on the transport properties and carbon dioxide solubility in trialkyltriazolium ionic liquids is described. The viscosities, diffusion coefficients, and conductivities of 15 1,2,4-trialkyl-1,2,3-triazolium bis(trifluoromethylsulfonyl)imide ILs are reported, and are found to be greatly reduced in ILs that incorporate multiple branched alkyl groups on the cation. The interrelationships among the transport properties are analyzed by comparing the deviations of the transport properties of each IL from Walden's Rule, the Stokes-Einstein equation, and the Nernst-Einstein equation. Preliminary evidence is given for a connection between the formation of polar and non-polar nanodomains within ILs, and the Nernst-Einstein deviation ratio. Henry's

Law constants for the solubility of carbon dioxide in the ILs are reported and found to be most strongly correlated to the molar volume of the IL; evidence supporting a relationship between the Nernst-Einstein deviation ratio and carbon dioxide solubility for a given IL is not found.

TABLE OF CONTENTS

TITLE PAGE	I
ABSTRACT.....	IV
TABLE OF CONTENTS	VI
LIST OF TABLES	IX
LIST OF FIGURES	XI
LIST OF EQUATIONS.....	XIII
LIST OF SYMBOLS AND ABBREVIATIONS.....	XIV
ACKNOWLEDGEMENTS	XV
1.0 INTRODUCTION.....	1
1.1 IONIC LIQUIDS	1
1.1.1 Structural Order in Alkyl-Functionalized ILs.....	3
1.1.2 ILs as Carbon Dioxide Capture Materials	4
2.0 METHODS AND MATERIALS	5
2.1 SELF DIFFUSION MEASUREMENT BY PFG-NMR.....	5
2.2 IONIC CONDUCTIVITY MEASUREMENT BY ELECTRICAL IMPEDANCE ANALYSIS	9
2.3 NERNST EINSTEIN DEVIATION PARAMETERS.....	11
2.4 TRIALKYLTRIAZOLIUM BIS(TRIFLUOROMETHYLSULFONYL)AMIDE ILS	14
3.0 STUDIES OF THE PHYSICAL AND TRANSPORT PROPERTIES OF TRIAALKYLTRIAZOLIUM BIS(TRIFLUOROMETHYLSULFONYL)IMIDES	16
3.1 INTRODUCTION	16

3.2	PHYSICAL PROPERTIES	17
3.2.1	IL Structures	17
3.2.2	Density and Molar Volume	19
3.3	TRANSPORT PROPERTIES	22
3.3.1	Results.....	22
3.3.2	Dependence of Viscosity on Alkyl Chain Length and Branching	23
3.3.3	Self-Diffusion.....	26
3.3.4	Stokes-Einstein Analysis	26
3.3.5	Ionic and Molar Conductivities.....	32
3.3.6	Walden Plot Analysis.....	32
3.3.7	Nernst-Einstein Deviation.....	35
3.4	NMR CHEMICAL SHIFT DATA	38
3.5	CARBON DIOXIDE SOLUBILITY DATA	40
3.5.1	Results.....	40
3.5.2	Statistical Correlation with Physical and Transport Parameters.....	41
3.5.3	Effect of Isomerization	44
4.0	CONCLUSIONS	45
5.0	EXPERIMENTAL	47
5.1	GENERAL.....	47
5.2	DENSITY AND VISCOSITY MEASUREMENTS.....	47
5.3	CARBON DIOXIDE SOLUBILITY MEASUREMENTS	48
5.4	MOLAR VAN DER WAALS VOLUME COMPUTATIONS	49
5.5	NMR EXPERIMENTS	49

5.5.1	Experimental Details	49
5.5.2	Representative ^1H and ^{19}F Spectra and Fits of Diffusion Data to Stejskal-Tanner Equation	50
5.5.3	^1H and ^{19}F NMR Chemical Shift Data of Neat ILs.....	57
5.6	ELECTRICAL IMPEDANCE SPECTROSCOPY	66
APPENDIX A: COMPLETE PARAMETERS OF LINEAR REGRESSION ANALYSES		68
BIBLIOGRAPHY		72

LIST OF TABLES

Table 1. Numbering of the ILs and Cation Structures.	18
Table 2. Density and Molar Volume of the ILs studied.	20
Table 3. Calculated Excess Molar Volumes and Fraction of Free Volume of ILs Studied.....	21
Table 4. Viscosity, Self-Diffusion, Conductivity, and Ionicity Ratios of the ILs Studied.	23
Table 5. Fitting Parameters for Correlations of Viscosity to Adjusted Alkyl Chain Length.....	24
Table 6. Comparison of Relative Hydrodynamic Radii of Isomeric ILs.	31
Table 7. Henry's Law Constants of Carbon Dioxide Solubility for the ILs Studied.....	41
Table 8. Statistical Significance of Molar Volume and Ionicity Parameters for K_H Determination.	43
Table 9. NMR chemical shift data for neat [Tz3n11][Tf ₂ N].	57
Table 10. NMR chemical shift data for neat [Tz4n11][Tf ₂ N].	57
Table 11. NMR chemical shift data for neat [Tz3n3n3n][Tf ₂ N].	58
Table 12. NMR chemical shift data for neat [Tz3n3n3i][Tf ₂ N].	58
Table 13. NMR chemical shift data for neat [Tz3i3i3i][Tf ₂ N].	59
Table 14. NMR chemical shift data for neat [Tz4n14n][Tf ₂ N].	59
Table 15. NMR chemical shift data for neat [Tz5n5n1][Tf ₂ N].	60
Table 16. NMR chemical shift data for neat [Tz4n4n4n][Tf ₂ N].	60
Table 17. NMR chemical shift data for neat [Tz4i4i4i][Tf ₂ N].	61
Table 18. NMR chemical shift data for neat [Tz8i3n1][Tf ₂ N].	61
Table 19. NMR chemical shift data for neat [Tz5n5n5n][Tf ₂ N].	62
Table 20. NMR chemical shift data for neat [Tz7i7n1][Tf ₂ N].	62

Table 21. NMR chemical shift data for neat [Tz7n7n3n][Tf ₂ N].	63
Table 22. NMR chemical shift data for neat [Tz8i8n1][Tf ₂ N].	64
Table 23. NMR chemical shift data for neat [Tz7n7n7n][Tf ₂ N].	65

LIST OF FIGURES

Figure 1. Representative examples of cation and anion structures used in ILs.	2
Figure 2. Pulse sequence and schematic representation of the effect of pulsed field gradients and diffusion on nuclear spins	8
Figure 3. A representative Nyquist plot.	10
Figure 4. Diagram of an equivalent circuit	11
Figure 5. Generalized structure of trialkyltriazolium cation and structure of the Tf ₂ N anion.	14
Figure 6. Plot of viscosity vs. n _{adj} for c _n values	25
Figure 7. Self-diffusion coefficient D vs. 1/ηr.	28
Figure 8. Experimental vs. calculated, r _{H+} /r _H ratios of the ILs.	30
Figure 9. Walden-type plot of conductivity and viscosity data.	34
Figure 10. Ionicity ratio vs. excess molar volume.	37
Figure 11. ¹ H shift of proton H5 and ¹⁹ F Chemical Shift of -CF ₃ vs. (v _m) ^{1/3}	39
Figure 12. ¹ H NMR spectrum of [Tz3n11][Tf ₂ N].	51
Figure 13. ¹⁹ F NMR spectrum of [Tz3n11][Tf ₂ N].	51
Figure 14. Fit of ¹ H (cation) diffusion data to Stejskal-Tanner equation for [Tz3n11][Tf ₂ N].	52
Figure 15. Fit of ¹⁹ F (anion) diffusion data to Stejskal-Tanner equation for [Tz3n11][Tf ₂ N].	52
Figure 16. ¹ H NMR spectrum of [Tz8i3n1][Tf ₂ N].	53
Figure 17. ¹⁹ F NMR spectrum of [Tz8i3n1][Tf ₂ N].	53
Figure 18. Fit of ¹ H (cation) diffusion data to Stejskal-Tanner equation for [Tz8i3n1][Tf ₂ N].	54
Figure 19. Fit of ¹⁹ F (anion) diffusion data to Stejskal-Tanner equation for [Tz8i3n1][Tf ₂ N].	54
Figure 20. ¹ H NMR spectrum of [Tz7n7n7n][Tf ₂ N]	55

Figure 21. ^{19}F NMR spectrum of $[\text{Tz7n7n7n}][\text{Tf}_2\text{N}]$ 55

Figure 22. Fit of ^1H (cation) diffusion data to Stejskal-Tanner equation for $[\text{Tz7n7n7n}][\text{Tf}_2\text{N}]$. 56

Figure 23. Fit of ^{19}F (anion) diffusion data to Stejskal-Tanner equation for $[\text{Tz7n7n7n}][\text{Tf}_2\text{N}]$. 56

LIST OF EQUATIONS

Equation 1	5
Equation 2	6
Equation 3	6
Equation 4	7
Equation 5	11
Equation 6	11
Equation 7	12
Equation 8	12
Equation 9	12
Equation 10	24
Equation 11	26
Equation 12	32

LIST OF SYMBOLS AND ABBREVIATIONS

Λ – molar conductivity

Λ_{imp} – molar conductivity measured by electrochemical impedance spectroscopy

Λ_{NMR} – theoretical molar conductivity calculated by Nernst-Einstein equation from self-diffusion coefficients

η - viscosity

σ – specific conductivity

ρ - density

CO_2 – carbon dioxide

D_+/D_- – self-diffusion coefficient of cation/self-diffusion coefficient of anion

IL – ionic liquid

NMR – nuclear magnetic resonance

PFG – pulsed field gradient

RTIL – room temperature ionic liquid

SANS – small-angle neutron scattering

SAXS – small-angle X-ray scattering

Tf_2N – bis(trifluoromethylsulfonyl)imide

Tz – triazolium

WAXS – wide-angle X-ray scattering

ACKNOWLEDGEMENTS

First and foremost, I would like to acknowledge my research director, Dr. Damodaran Krishnan Achary, for his guidance and instruction throughout my time at the University of Pittsburgh. I am very grateful to him for giving me the opportunity to work on this and other interesting research projects. In addition, I would like to express my thanks to him for the equally-important education in NMR and in research which I received under his guidance as my supervisor in my staff position as NMR Facility Assistant.

I would also like to thank my committee members, Dr. Dennis Curran, Dr. Sunil Saxena, and Dr. Stephen Weber, for their guidance as I completed my masters studies and research, and for their helpful comments and discussions during the revision of this thesis. Without Dr. Curran's encouragement to continue my education in particular, I probably would not have begun work on a Master's Degree.

This collaborative project would not have been possible without the researchers who participated, and the National Energy Technology Laboratory: Dr. James Mao, Dr. Yougang Mao, from the Damodaran group, and Dr. Mike Lartey, Dr. Eric Albenze, and Dr. Hunaid Nulwala of NETL.

Throughout my time in the Department of Chemistry I have relied on the support of nearly all of my fellow staff members in the department, but a number deserve special recognition in connection with this thesis: Lori Neu, who created and helped to design glassware for the conductivity measurements, Jeff Sicher and Tom Gasmire, who constructed and helped to design our group's dry box, and Dave Emala, who gave invaluable advice about temperature

control and constructed adapters and electronics components for use with our impedance analyzer.

Finally I would like to acknowledge all the past and current users of the NMR Facility during my time in the Department of Chemistry. Their questions and discussions with me about NMR provided an unofficial education of their own during my time in the NMR Facility. It has been a privilege to serve such a friendly, bright, and patient group of people; I hope I have been as useful to them during my time here as they have been to me.

1.0 INTRODUCTION

1.1 IONIC LIQUIDS

Room temperature ionic liquids (RTILs or ILs) are the class of salts with melting points of 100 °C or lower.¹ RTILs generally consist of a bulky organic cation and a smaller organic or inorganic anion; examples of common cations and anions for ILs are shown in Figure 1 below.² They are able to remain liquid at lower temperatures than conventional salts due to their bulky and asymmetrical structures, which frustrate efficient crystal packing.¹ The presence of the Coulomb forces among ions imparts a number of features to ILs that are absent in most molecular liquids, including the formation of local heterogeneities and intermediate-range ordering within the solution,³ ionic conductivity, and wide electrochemical windows.⁴

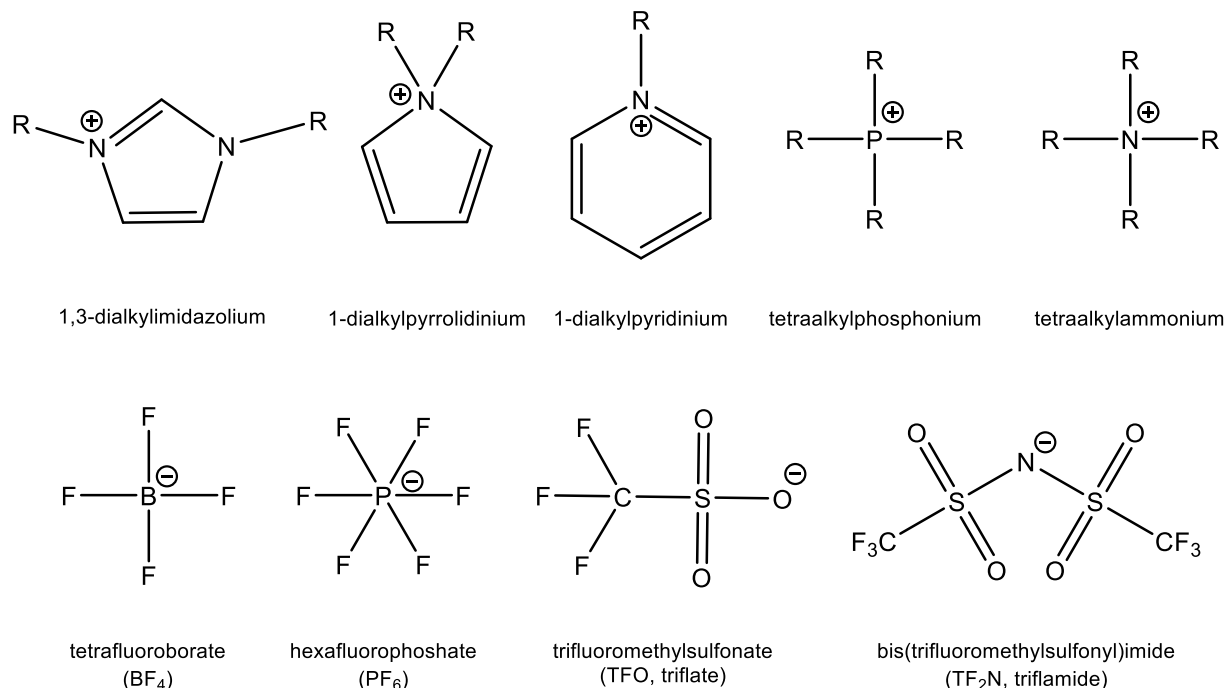


Figure 1. Representative examples of cation and anion structures used in ILs. –R = alkyl group.

The use of ILs as replacements for molecular solvents has attracted great attention in recent years. As a class, they exhibit many properties that make their use environmentally favorable, such as their very low volatility and non-flammability. The potential to tailor ILs to produce specific physical or transport properties, or to enhance specific interactions with solutes, through the choice of ionic structures, has led to the designation of ILs as “designer solvents”.⁵ ILs are already in use in a number of commercial processes including acid-scavenging⁶ and compressed gas handling,⁷ and show great future promise in the processing of cellulose,⁸⁻¹¹ carbon dioxide,¹²⁻¹⁷ and spent nuclear materials,¹⁸ among many other applications.

It is estimated that 10⁶ unique ILs could be produced through combination and functionalization of existing cation and anion structures alone.¹⁹ Given the enormous number of possible ILs, there is a great impetus to systematically study the relationships among ionic

structures, intermediate-range ordering of the structures, and bulk IL properties, in order to more rationally design task-specific ILs. Studies into the specific interactions of ILs with molecular solutes are also critical to developing the use of ILs as solvents. The research presented in this work details the systematic study of a specific family of ILs, the 1,2,4-trialkyl-1,2,3-triazolium bis(trifluoromethylsulfonyl)imides, in an attempt to understand the role that ion structure and inter-ionic interactions play in determining these ILs' physical and transport properties, and abilities to solvate carbon dioxide.

1.1.1 Structural Order in Alkyl-Functionalized ILs

Critical to the understanding of IL self-interactions and interactions with solutes are the unusual behaviors of these compounds at the ionic level due to the density of electrostatic charges. The existence of local ordering within ILs was first predicted by molecular dynamics simulations,²⁰⁻²⁵ and later confirmed by small-angle X-ray scattering (SAXS), wide-angle X-ray scattering (WAXS), and small-angle neutron scattering (SANS) experiments in alkyl-functionalized imidazolium,²⁶⁻³³ ammonium,³⁴ and piperidinium³⁵ ILs. In ILs with short alkyl chains, the Coulomb forces are dominant, and alternation of charge creates a structure similar to a disordered lattice.²⁶ As the alkyl chain length increases, the tails can no longer be incorporated into the interstitial spaces of the disordered lattice, and the ions begin to arrange themselves into polar and non-polar nanodomains. Such behavior has only been observed in a few molecular solvents, namely *n*-alkyl alcohols.²⁷ The size of the nanodomains formed, as well as the specific alkyl chain lengths at which nanodomains begin to form in a given IL family, are influenced by the both the structure of the cation and the size of the anion.³⁰

1.1.2 ILs as Carbon Dioxide Capture Materials

One of the solutes whose interactions with ILs have attracted great attention in recent years is carbon dioxide (CO₂). The development of new materials for the post-combustion capture of CO₂ from industrial flue gases is a critical element of mitigating the buildup of this greenhouse gas in the atmosphere. The low volatility and high thermal stabilities of ILs make them especially attractive potential candidates for flue gas applications.³⁶ However, much work remains to be done in the optimization of ion structures for CO₂ sorbent ILs, as those developed thus far suffer from high viscosities compared to conventional solvents, and their CO₂ uptake capacities are not yet greater than conventional CO₂ capture solvents.¹² Both ILs that complex chemically with CO₂ and ILs that act only as physical sorbents have been reported; within the context of this thesis, only physically absorbing ILs will be discussed.

The absorption of CO₂ into ILs produces minimal volume expansion, suggesting that the CO₂ is accommodated within the existing free volume of the liquid. Thus far, a number of studies have found that the most important predictor of CO₂ solubility in ILs is the total molar volume of the liquid.^{37,38} However, evidence of an anion effect has also been reported from studies of specific cation families, mainly the 1,3-dialkylimidazoliums. While both varying alkyl chain length and varying the choice of anion change the molar volume of the liquid, the effect of the latter is much greater on the CO₂ solubility.³⁹ In general, anions with greater steric bulk, greater conformational flexibility, and more distributed charges tend to promote carbon dioxide solubility within the IL.³⁸ Fluorinated anions outperform their non-fluorinated analogues.⁴⁰

The solubility of gases in ILs is thus determined by the free volume available to accommodate the gas molecule within the liquid, the flexibility of the cation and anion structures within the IL, and the strength of specific favorable or unfavorable IL-gas interactions.³⁸

2.0 METHODS AND MATERIALS

Our methodology for studying the underlying solution organization and understanding the interactions among ionic properties was the study of three of their transport properties: viscosity, self-diffusion, and ionic conductivity. The theoretical relationships between these properties for ions in the ideal case of infinite dilution are well established; however, in the purely ionic environment of an IL, the strong Coulomb interactions and the presence of nanoscale heterogeneities will cause deviations from the behavior predicted by such relationships. When such deviations are compared among a class of ILs, the magnitudes of these deviations from ideality, as well as their relationships to the physical properties of the ILs, will give insights into the nature of the interactions among ions in the solution.

2.1 SELF DIFFUSION MEASUREMENT BY PFG-NMR

The self-diffusion coefficient is the diffusion coefficient of a species in the absence of a chemical potential gradient. In isotropic homogeneous systems it is related to the root-mean-square displacement of the particle by the Einstein equation

$$\sqrt{\langle x^2 \rangle} = \sqrt{nDt_D} \quad (1)$$

where x is displacement, D is the diffusion coefficient, t_D is diffusion time, and n is 2, 4, or 6 for a one-, two-, or three-dimensional system, respectively.⁴¹

While the first measurements of the self-diffusion coefficients of high-temperature inorganic molten salts and aluminochlorate ILs were carried out by means of measuring the diffusion of radioactive isotopomers of the ions through a capillary,⁴²⁻⁴⁵ the low melting temperatures of RTILs allow the use of the pulsed-field-gradient NMR (PFG-NMR) method for this purpose. The NMR technique has the advantages of much greater ease of use, as well as not requiring corrections for isotope effects.

The basis of pulsed-field gradient NMR is the brief application of a magnetic gradient along the z -axis to apply phase labeling to nuclei dependent on their location the NMR tube. The most basic PFG pulse sequence is illustrated in Figure 2.⁴⁶ In the rotating frame, the position-dependence of the phase shift caused by the gradient pulse is expressed as

$$\phi(z) = \gamma\delta\sigma g(z) \quad (2)$$

where γ is the gyromagnetic ratio of the nucleus observed, δ is the length of the gradient pulse, $g(z)$ is the magnetic field strength of the gradient at position z , and σ is a correction factor for the shape of the gradient pulse. After application of the gradient, the a diffusion time of $\Delta/2$ is passed, before the sign of the phase shift is reversed by the application of a 180° pulse and a second gradient, equal to the first, is applied. A delay of $\Delta/2$ is again passed to allow the spin echo to refocus. The final phase shift of the nucleus will thus be given by the expression

$$\Delta\phi = \phi(z_f) - \phi(z_i) = \gamma\delta\sigma \left(g(z_f) - g(z_i) \right) \quad (3)$$

Thus, as pictured in Figure 2 below, the effect of self-diffusion will be to create spread in the distribution of phase angles of the nuclei, reducing the signal intensity. The relationship

between the diffusion coefficient of a species and the attenuation of the signal intensities for the resonances of the species is given by the Stejskal-Tanner equation^{47,48}

$$I = I_0 e^{-(\gamma^2 \delta^2 g^2 \sigma^2 \Delta D)} \quad (4)$$

where I is the observed intensity, I_0 is the intensity at zero gradient strength, Δ is the free diffusion time, and all other symbols are as in Equation 3. By fitting a series of experiments obtained with systematically varied δ , Δ , or g , it is possible to obtain the diffusion coefficient through fitting of the signal intensities to Equation 4. In modern usage, it is the gradient strength g is varied while the free-diffusion time Δ and gradient pulse width δ are kept constant, to avoid the need for introducing corrective factors for the intensity lost due to T_1 and T_2 relaxation of the nuclei.

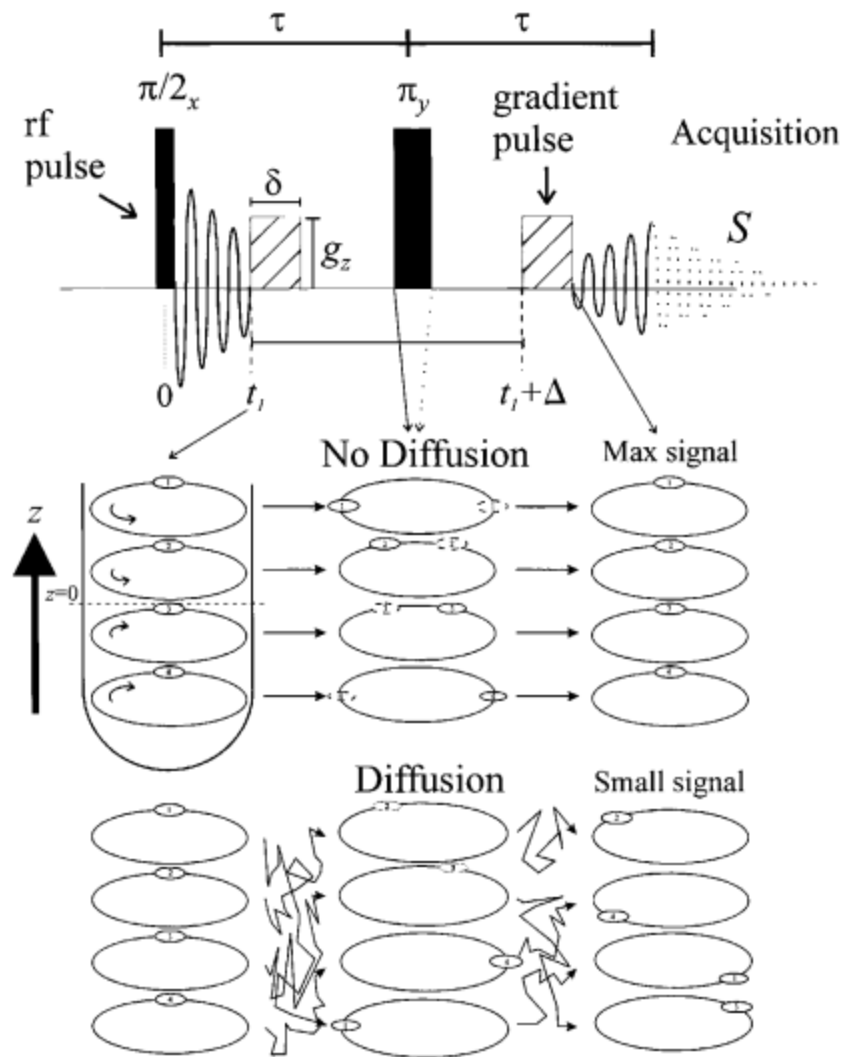


Figure 2. Pulse sequence and schematic representation of the effect of pulsed field gradients and diffusion on nuclear spins. Reproduced from Reference 38 with permission.

2.2 IONIC CONDUCTIVITY MEASUREMENT BY ELECTRICAL IMPEDANCE ANALYSIS

The measurement of the conductivity of an electrolyte solution must be conducted using an alternating potential to avoid polarization of the solution. However, such measurements are complicated by the fact that the response of an electrolyte solution to an alternating potential is not purely resistive; but instead are represented by the complex, frequency dependent quantity impedance. Additional complications arise from the fact that the electrode-electrolyte interface itself exhibits an additional capacitive response to the alternating potential.⁴⁹

The problem of frequency dependence of the observed resistance can be overcome through the use of a frequency response analyzer in conjunction with the voltage source, which is capable of measuring both the magnitude of a current and the phase difference between the applied voltage and the current, and thus is able to separate the magnitude and phase components of the complex impedance, Z .⁵⁰ These polar data are then transformed into their Cartesian representation and displayed visually on the so-called Nyquist plot, $-\text{Im}(Z)$ vs. $\text{Re}(Z)$. Some software packages also referred to these axes as, Z'' and Z' , respectively. On such a plot, the point of lowest phase shift, i.e. the point with the smallest magnitude of $-\text{Im}(Z)$, represents the resistance of the liquid;⁵¹ an example of such a plot is shown in Figure 3 below.

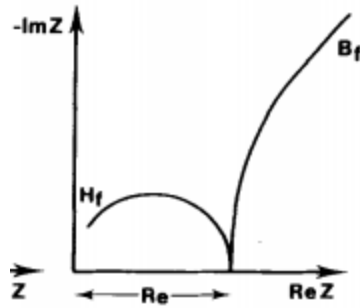


Figure 3. A representative Nyquist plot. The diameter of the loop near the origin represents the electrical resistance of the electrolyte solution. Reproduced with permission from Reference 51.

The explanation of the coincidence of the minimum of $-\text{Im}(Z)$ with the resistance of the electrolyte can be understood by the theoretical equivalent electrical circuit of an electrolyte solution.⁵² As shown in Figure 4, the solution is represented as an RC circuit having a geometrical capacitance C_g and an electrolyte resistance R_e ; in series with R_e the electrode effects are represented as a parallel circuit consisting of the a capacitance resulting from the local polarization of the electrodes C_d and the Faradic impedance arising from the electrode-solution interface. The capacitance C_d is very small; such that the dominant impedance response at higher frequencies is dominated by the electrolyte. Thus, the minimum of $-\text{Im}(Z)$ represents the point at which the frequency is less than the time constant of the solution equivalent circuit, but greater than that of the electrode equivalent circuit; i.e. the capacitor C_g is acting as an open circuit and C_d as a closed circuit; thus, the only contribution to impedance across the cell is the electrolyte resistance R_e .

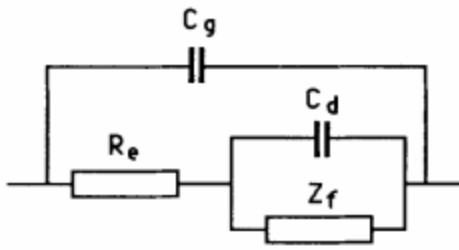


Figure 4. Diagram of an equivalent circuit of an electrolyte solution and cell capacitance. The elements of the outer circuit represent behavior arising from response of ions in the bulk solution to an applied current, while the inner circuit represents electrode surface processes. Reproduced with permission from Reference 50.

The conductivity is then calculated from resistance by the relation

$$C = \frac{k}{R} \quad (5)$$

where k is a correction factor for the surface area and spacing of the electrodes that is calibrated for a specific cell using an electrolyte solution of known conductivity.

2.3 NERNST EINSTEIN DEVIATION PARAMETERS

The limiting ionic conductivity of an electrolyte species is related to its self-diffusion coefficient by the Nernst-Einstein relationship⁴⁹

$$\lambda = \frac{nF^2z^2D}{RT} \quad (6)$$

where λ is the ionic conductivity, n is the number density, R is the gas constant, F is the Faraday constant, z is the valence of the ion, and D is the self-diffusion coefficient of the species.

At infinite dilution, the Kohlrausch Law of Independent Migration states that the specific conductivity of a solution is the sum of the contributions of the specific conductivities of each ionic species;⁴⁹ that is for a binary electrolyte with both species univalent,

$$\lambda = \lambda_+ + \lambda_- \quad (7)$$

where λ is the specific conductivity of the electrolyte, λ_+ is the specific conductivity of the cation, and λ_- is the specific conductivity of the anion. Combining Equations 6 and 7, and converting the ionic conductivity to molar conductivity by the conversion $\Lambda = \frac{N_A \lambda}{n}$ in terms of the molar conductivity, we obtain

$$\Lambda = \frac{F^2(D_+ + D_-)}{RT} \quad (8)$$

where Λ is the molar conductivity and all other symbols are as in Equation 7.

For ILs, the molar conductivity measured experimentally is always less than that predicted by the Nernst-Einstein equation. A number of equivalent parameters to describe this deviation have been developed. Researchers of molten inorganic salts in the mid-20th century traditionally reported deviation from Nernst-Einstein behavior using a modified Nernst-Einstein equation^{42,43,53}

$$\Lambda = \frac{F^2(D_+ + D_-)}{RT} (1 - \Delta) \quad (9)$$

An alternative method developed by Watanabe and coworkers of reporting such deviations has become widespread in the study of modern RTILs, in which the quantity is expressed as the ratio

$\frac{\Lambda_{imp}}{\Lambda_{NMR}}$,⁵⁴⁻⁵⁸ with the subscripts referring to the experimental techniques used; they were also the

first to apply the name “ionicity” to this parameter. The Δ and $\frac{\Lambda_{imp}}{\Lambda_{NMR}}$ parameters are trivially

related by the expression $\frac{\Lambda_{imp}}{\Lambda_{NMR}} = (1 - \Delta)$.

The major origin of the deviation is the non-independence of the motions of cations and anions, is simultaneous correlated motion of oppositely charged ions in the same direction. The correlated motion of an anion and cation will contribute to the measured diffusion, but will have zero contribution to the net current. Two models for the mechanism of the correlated diffusion of anion and cation motion have been proposed; in the first, the IL is considered to be an incompletely dissociated electrolyte; that is, the solution is assumed to consist of individual anions and cations in equilibrium with long-lived ion pairs that constitute a third, chemically distinct, species in the solution.⁵⁹ The second is the paired-vacancy mechanism. In this model, the structure of the IL is considered to be lattice-like, and the diffusion of ions is considered to occur by a jump-like process into cavities that arise from the thermal fluctuation of the free volume within the liquid. If the dimensions of the cavity formed are great enough, an ion may jump into a vacancy with one of the counter-ions of its solution shell.⁴³

Thus far, spectroscopic studies of ILs have detected specific interactions between anions and cations interactions, but not the presence of long-lived ion pairs. No separate resonances identifiable as belonging to paired ions can be detected by 1D NMR experiments; nor do the diffusion data indicate multiple diffusion coefficients. A terahertz dielectric spectroscopy study of the IL 1-methyl-3-butylimidazolium tetrafluoroborate failed to find evidence for reorientation of stable ion pairs.⁶⁰ Additionally, in one case ILs were reported to show increased deviation from Nernst-Einstein behavior at high temperatures,^{53,55} which is consistent with the paired-vacancy mechanism, but contrary to the expected result of the ionic association hypothesis. However, even if not directly responsible for the decrease in conductivity, it is expected that favorable cation-anion interactions will reduce the measured ionicity ratio by increasing the energy required for an ion to diffuse away separately from its partner. Increased free volume and

flexibility of free volume will also decrease ionicity, as the formation of cavities of suitable size to accommodate a paired jump will increase.

2.4 TRIALKYLTRIAZOLIUM BIS(TRIFLUOROMETHYLSULFONYL)AMIDE ILS

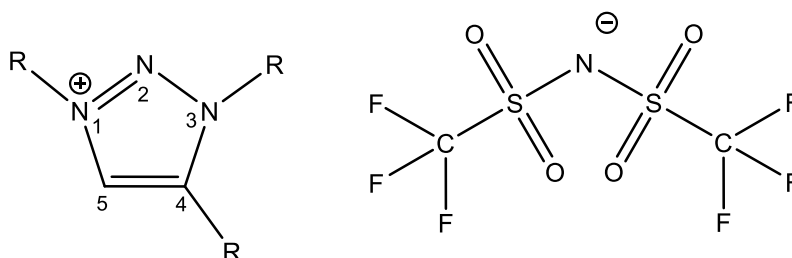


Figure 5. Generalized structure of trialkyltriazolium cation and structure of the Tf₂N anion. Atom numbering on the cation will be used throughout. R = alkyl group.

In order to systematically study the effects of cation functionalization on the properties of ILs, it is desirable to have a cation structure that can be simply and efficiently synthesized with a wide variety of functional groups. To this end, the CO₂ Capture Group at the NETL labs has been studying the development of ILs based on the 1,2,4-trialkyl-1,2,3-triazolium cation.⁶¹⁻⁶³ The structure of the cation is shown in Figure 5 below. This family of cations can be conveniently synthesized via the atom efficient and high-yield Copper(I)-catalyzed Azide-Alkyne Cycloaddition reaction.⁶¹ The triazolium structure is also convenient in that it is similar to the best-studied family of cations, the 1,3-disubstituted imidazoliums, for which physical properties and transport properties have been extensively reported.

The bis(trifluoromethylsulfonyl)imide (Tf₂N) anion, has been found to promote the solubility of CO₂ in ILs; this property has been attributed to its conformational flexibility,

fluorination, and non-coordinating nature.³⁹ ILs based on the Tf₂N anion, particularly those with alkyl-functionalized cations, tend to be immiscible in water, a desirable property for flue gas applications.⁶⁴ Use of the Tf₂N anion avoids problems of undesired acid-base reactions inherent to other anions; it does not produce acid breakdown products in the presence of water as purely inorganic ions like tetrafluoroborate⁶⁵ do, nor, as the conjugate base of a superacid, does it deprotonate Lewis acid cations or solutes, as more basic anions like acetate may.⁶⁶

3.0 STUDIES OF THE PHYSICAL AND TRANSPORT PROPERTIES OF TRIALKYLTRIAZOLIUM BIS(TRIFLUOROMETHYLSULFONYL)IMIDES

3.1 INTRODUCTION

In this chapter, the self-diffusion coefficients, ionic conductivities, and ionicity ratios are presented for 15 novel trialkyltriazolium bis(trifluoromethylsulfonyl)imide ILs. The relationships among these transport properties, and the densities, viscosities, and Henry's Law constants for carbon dioxide solubility are discussed. The results are discussed in terms of possible relationships with the free molar volume in the ILs, which is calculated using computationally-determined ionic volumes and experimentally determined molar volumes.

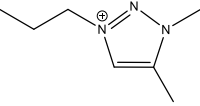
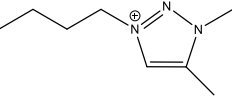
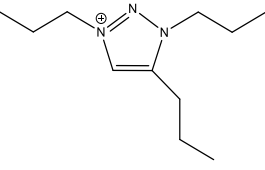
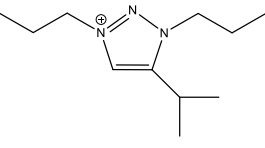
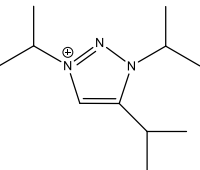
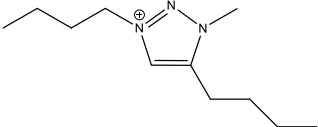
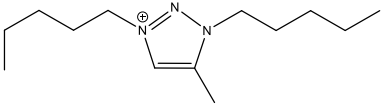
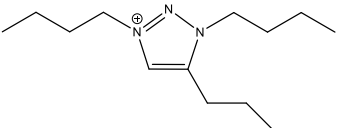
The work presented in this chapter was carried out as a collaborative effort between the Damodaran Group at the University of Pittsburgh and the Carbon Capture Group at the National Energy Technology Laboratory at Pittsburgh, PA. In cases where experimental work was performed by a researcher other than the author, the name and affiliation of the researcher are given at the beginning of the section.

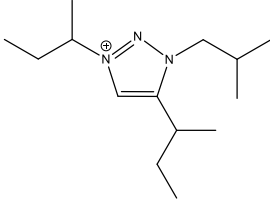
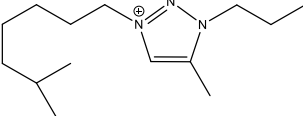
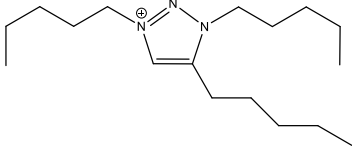
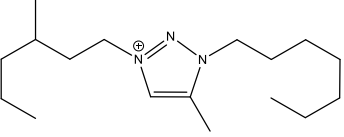
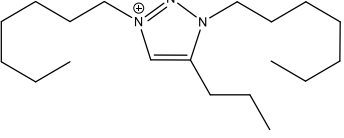
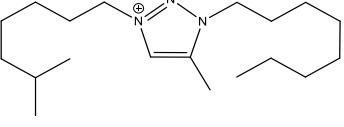
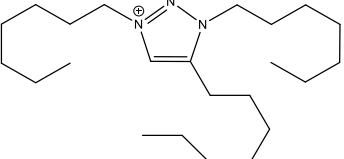
3.2 PHYSICAL PROPERTIES

3.2.1 IL Structures

Fifteen trialkyltriazolium Tf₂N ILs were prepared by Dr. Michael Lartey at the Pittsburgh NETL Laboratory. For convenience, a system of short names similar to those found in the literature for di- and trialkylimidazolium ILs has been developed for this family of cations, in which the letters “Tz” indicate the triazolium ring backbone, and the three numbers following indicate the number of carbons contained in the 1, 3, and 4 alkyl chains, respectively. The letter “n” following a number designates an *n*-alkyl group; an “i” indicates a methyl group branching on a given chain. The structures of the ions and molar weights of the resulting ILs are shown in Table 1 below.

Table 1. Numbering of the ILs and Cation Structures.

Compound	Cation	Cation Structure	Short Name	Molar Weight / g mol^{-1}
1	1-propyl-3,4-dimethyl-1,2,3-triazolium		[Tz3n11] [Tf ₂ N]	420.39
2	1-butyl-3,4-dimethyl-1,2,3-triazolium		[Tz4n11] [Tf ₂ N]	434.41
3	1,3,4-tripropyl-1,2,3-triazolium		[Tz3n3n3n] [Tf ₂ N]	476.49
4	1,3-dipropyl-4-(2-methyl)ethyl-1,2,3-triazolium		[Tz3n3n3i] [Tf ₂ N]	476.49
5	1,3,4-tri(2-methyl)ethyl-1,2,3-triazolium		[Tz3i3i3i] [Tf ₂ N]	476.49
6	1,4-dibutyl-3-methyl-1,2,3-triazolium		[Tz4n14n] [Tf ₂ N]	476.49
7	1,3-dipentyl-4-methyl-1,2,3-triazolium		[Tz5n5n1] [Tf ₂ N]	504.55
8	1,3,4-tributyl-1,2,3-triazolium		[Tz4n4n4n] [Tf ₂ N]	518.57

9	1,4-di(1-methyl)propyl-3-(2-methyl)-1,2,3-triazolium		[Tz4i4i4i] [Tf ₂ N]	518.57
10	1-(6-methyl)heptyl-3-propyl-4-methyl-1,2,3-triazolium		[Tz8i3n1] [Tf ₂ N]	518.57
11	1,3,4-tripentyl - 1,2,3-triazolium		[Tz5n5n5n] [Tf ₂ N]	560.65
12	1-(2-methyl)hexyl-3-heptyl-4-methyl-1,2,3-triazolium		[Tz7i7n1] [Tf ₂ N]	560.65
13	1,3-diheptyl-4-propyl-1,2,3-triazolium		[Tz7n7n3n] [Tf ₂ N]	588.71
14	1-(6-methyl)heptyl-3-octyl-4-methyl-1,2,3-triazolium		[Tz8i8n1] [Tf ₂ N]	588.71
15	1,3,4-triheptyl - 1,2,3-triazolium		[Tz7n7n7n] [Tf ₂ N]	644.81

3.2.2 Density and Molar Volume

Density data were provided by Dr. Michael Lartey at the NETL Laboratory in Pittsburgh, PA. Details of the experimental conditions are provided in the experimental section. The data are

listed in Table 2 below, along with the total number of carbon atom units incorporated in the ILs alkyl chains, n , and the molar volumes v_m of the ILs.

Table 2. Density and Molar Volume of the ILs studied.

IL	Cation	n	Density^a / g mL⁻¹	Molar Volume^b / cm³ mol⁻¹
1	Tz3n11	5	1.4723	285.53
2	Tz4n11	6	1.4480	300.01
3	Tz3n3n3n	9	1.3663	348.74
4	Tz3n3n3i	9	1.3466	353.85
5	Tz3i3i3i	9	1.3458	354.06
6	Tz4n14n	9	1.3630	349.59
7	Tz5n5n1	11	1.3149	383.71
8	Tz4n4n4n	12	1.2992	399.15
9	Tz4i4i4i	12	1.2828	404.25
10	Tz8i3n1	12	1.3112	395.49
11	Tz5n5n5n	15	1.2430	451.05
12	Tz7i7n1	15	1.2226	458.57
13	Tz7n7n3n	17	1.2259	480.23
14	Tz8i8n1	17	1.1983	491.29
15	Tz7n7n7n	19	1.1579	556.88

^a Density data provided by Dr. Michael Lartey. Error of the density measurement is $\pm 0.5\%$. ^b Calculated from density values.

The van der Waals volumes (v_{vdw}) of the ions were calculated from the volume of the electron density isosurfaces of the ions by Dr. James Mao. The excess molar volume (v_{excess}) was calculated from the molar volume (v_m) as $v_{excess} = v_m - v_{vdw}$ and fraction free volume (FFV) was calculated as $FFV = \frac{v_{excess}}{v_m}$. These values are listed in Table 3 below.

Table 3. Calculated Excess Molar Volumes and Fraction of Free Volume of ILs Studied.

IL	Cation	v_{vdW}^a / $\text{cm}^3 \text{mol}^{-1}$	v_{excess}^b / $\text{cm}^3 \text{mol}^{-1}$	FFV ^b
1	Tz3n11	207	78.53	0.275
2	Tz4n11	219	81.01	0.270
3	Tz3n3n3n	254	94.74	0.272
4	Tz3n3n3i	254	99.85	0.282
5	Tz3i3i3i	254	100.06	0.283
6	Tz4n14n	254	95.59	0.273
7	Tz5n5n1	278	105.72	0.275
8	Tz4n4n4n	289	110.15	0.276
9	Tz4i4i4i	290	114.25	0.282
10	Tz8i3n1	290	105.49	0.267
11	Tz5n5n5n	325	133.57	0.291
12	Tz7i7n1	325	126.05	0.279
13	Tz7n7n3n	349	142.29	0.290
14	Tz8i8n1	349	131.23	0.273
15	Tz7n7n7n	396	160.88	0.289

^a van der Waals volumes provided by Dr. James Mao. ^b Calculated from v_m and v_{vdW} as detailed above.

As observed previously for dialkylimidazolium ILs, the density and molar volumes of the solution are to a good approximation linearly related to the total number of methylene units incorporated in the cation alkyl chains.⁶⁷ Linear regression over the whole data set produced the empirical relationship $\rho = -0.0197(\pm 9 \times 10^{-5})n + 1.5412(\pm 0.007)$, where ρ is density. The coefficient of determination R^2 for the fit was 0.9571. The decrease in density with increasing alkyl chain length can be attributed to the greater flexibility of the alkyl chains compared to the triazolium cores, as well as the weaker nature of the van der Waals interactions between the alkyl chains as compared to the Coulomb interactions of the anion and cationic triazolium group.

Among isomer pairs in which varied in their number of branched alkyl chains but not in the total number of carbon atoms of each chain, the density of the branched isomers were 0.02 g/mol lower than the *n*-alkyl isomers, whether one or three branched chains were included. Zheng et al.⁶⁷ showed that for isomeric dialkylimidazolium cations with a total number of carbons *n*, density was greater for ILs having the $C_{n-1}C_1$ isomer than the corresponding $C_{n/2}C_{n/2}$

isomer.⁶⁷ Although the presence of a third alkyl substitution makes such a comparison between trialkyltriazolium cations more complicated, the enhanced packing of longer alkyl chains is illustrated by the greater density of [Tz4n14n][Tf₂N](**6**) compared to [Tz3n3n3n][Tf₂N](**3**).

Isomeric cations showed little difference among their calculated v_{vdw} values; the differences in v_{excess} among isomeric ILs were therefore equal to their differences in their v_{m} , with branched cations ILs having larger v_{m} and v_{excess} values than their straight-chain counterparts. While the substitution of one propyl group for an isopropyl group in [Tz3n3n3n](**3**) and [Tz3n3n3i](**4**) increased the molar volume by $5 \text{ cm}^3 \text{ mol}^{-1}$, further substitution of all three propyl groups for isopropyl groups to give [Tz3i3i3i](**9**) increased molar volume by less than $1 \text{ cm}^3 \text{ mol}^{-1}$. The increase in v_{vdw} and v_{m} with the addition of branching was larger for the longer alkyl chain cations, with molar volume increasing $7.5 \text{ cm}^3 \text{ mol}^{-1}$ between [Tz5n5n5n](**11**) and [Tz7i7n1](**12**) and $11 \text{ cm}^3 \text{ mol}^{-1}$ between [Tz7n7n3n](**13**) and [Tz8i8n1](**14**).

3.3 TRANSPORT PROPERTIES

3.3.1 Results

The values of viscosity (η), self-diffusion coefficients of the cation (D_+) and anion (D_-), specific conductivity (σ), molar conductivity (Λ), and ionicity ratio for the ILs studied are listed in Table 4 below. The self-diffusion coefficients of the cation and anion were measured at $30 \text{ }^\circ\text{C}$ by PFG-NMR self-diffusion measurements. The ionic conductivities of the ILs were measured at $30 \text{ }^\circ\text{C}$ by electrical impedance spectroscopy. Viscosity data at $22 \text{ }^\circ\text{C}$ were provided by Dr. Michael Lartey at the NETL Laboratory in Pittsburgh, PA. Details of the experimental

conditions for viscosity, self-diffusion, and conductivity measurements may be found in the experimental section.

Table 4. Viscosity, Self-Diffusion, Conductivity, and Ionicity Ratios of the ILs Studied.

IL	Cation	η^a / cP (22 °C)	D_+ / $10^{-11} \text{ m}^2 \text{ s}^{-1}$ (30 °C) ^b	D_- / $10^{-11} \text{ m}^2 \text{ s}^{-1}$ (30 °C) ^b	σ / 10^{-1} S m^{-1} (30 °C) ^c	Λ^d / $10^{-5} \text{ S m}^2 \text{ mol}^{-1}$ (30 °C)	Ionicity Ratio ^d
1	Tz3n11	54.5	3.82	2.80	5.22	14.9	0.61
2	Tz4n11	57.6	3.47	2.90	4.51	13.5	0.58
3	Tz3n3n3n	57.6	2.58	2.76	3.19	11.1	0.57
4	Tz3n3n3i	66.1	2.36	2.51	2.77	9.82	0.55
5	Tz3i3i3i	103.5	1.73	1.74	2.14	7.56	0.59
6	Tz4n14n	74.4	2.18	2.27	2.18	7.61	0.46
7	Tz5n5n1	69.6	2.11	2.45	1.96	7.53	0.45
8	Tz4n4n4n	72.0	1.85	2.23	1.79	7.16	0.48
9	Tz4i4i4i	214.5	0.67	0.85	0.88	3.42	0.63
10	Tz8i3n1	79.3	1.68	2.02	1.57	6.19	0.45
11	Tz5n5n5n	92.4	1.29	1.65	1.05	4.72	0.44
12	Tz7i7n1	106.4	1.26	1.61	0.93	4.28	0.40
13	Tz7n7n3n	110.8	1.26	1.56	0.79	3.78	0.36
14	Tz8i8n1	130.3	0.94	1.22	0.68	3.36	0.42
15	Tz7n7n7n	140.1	0.81	1.04	0.39	2.17	0.32

^a Viscosity data provided by Dr. Michael Lartey of NETL. Error of the viscosity measurements was $\pm 2\%$. ^b Error of the diffusion measurements was $\pm 3\%$. ^c Error of the conductivity measurements was $\pm 4\%$. ^d Calculated from ionic conductivity and molar volume. ^e Calculated from molar conductivity and self-diffusion coefficients by Equations 8 and 9.

3.3.2 Dependence of Viscosity on Alkyl Chain Length and Branching

As shown in Table 4 above, the viscosity of the ionic trialkyltriazolium ILs increased with increasing alkyl chain length, as has been observed for other alkyl-functionalized ILs.⁶⁸ Such behavior can be rationalized on the basis of the increased alkyl-alkyl interactions. Combined SAXS and viscosity studies^{33,67} of dialkylimidazolium ILs have found that the viscosities of ILs are closely related to the size of the non-polar domains formed. From the SAXS studies, it has been demonstrated that cations in which all alkyl chains are shorter than three carbon units do not participate in the formation of the non-polar domains, due to the steric

hindrance of the anion.^{28,33} A SAXS investigation on isomeric dialkylimidazolium ILs that, like the trialkyltriazolium ILs in this study varied only in the distribution of $-\text{CH}_2-$ units between their alkyl chains, showed that for two cations with a given number of methylene units n , the viscosity is greater for the C_{n-1}C_n isomer than for the corresponding $\text{C}_{n/2}\text{C}_{n/2}$ isomer.

The viscosities of the nine trialkyltriazolium ILs in this study whose cations were functionalized with only n -alkyl chains were fitted to a linear regression using their n parameter. Due to the non-participation of the $-\text{CH}_2-$ units α and β to the triazolium ring in van der Waals interactions, several adjusted total alkyl chain length n_{adj} were tested in the linear regression. The method of calculating the adjusted total chain length is shown in equation 10 below

$$n_{adj} = n_{1adj} + n_{2adj} + n_{4adj} \begin{cases} n_{xadj} = n_x - c_n, & \text{if } n_x \geq c_n \\ n_{xadj} = 0, & \text{if } n_x < c_n \end{cases} \quad (10)$$

where n_1 , n_2 , and n_4 refer to the alkyl chains at the 1, 2, and 4 positions of the cation, respectively. Values of c_n between 0 and 4, corresponding to minimum chain lengths from methyl to pentyl, were evaluated. The fittings for the regressions are shown in Figure 6 below; results of the fittings are summarized in Table 5.

Table 5. Fitting Parameters for Correlations of Viscosity to Adjusted Alkyl Chain Length.

Minimum Chain Length	Cutoff Parameter	Slope	Standard Error Slope	Intercept	Standard Error Intercept	R^2
Methyl	$c_n = 0$	5.25	0.615	19.8	7.78	0.826
Ethyl	$c_n = 1$	5.24	0.615	35.6	6.12	0.900
Propyl	$c_n = 2$	6.10	0.516	42.3	3.96	0.946
Butyl	$c_n = 3$	6.98	0.510	53.1	2.81	0.959
Pentyl	$c_n = 4$	8.45	0.883	62.2	3.34	0.919

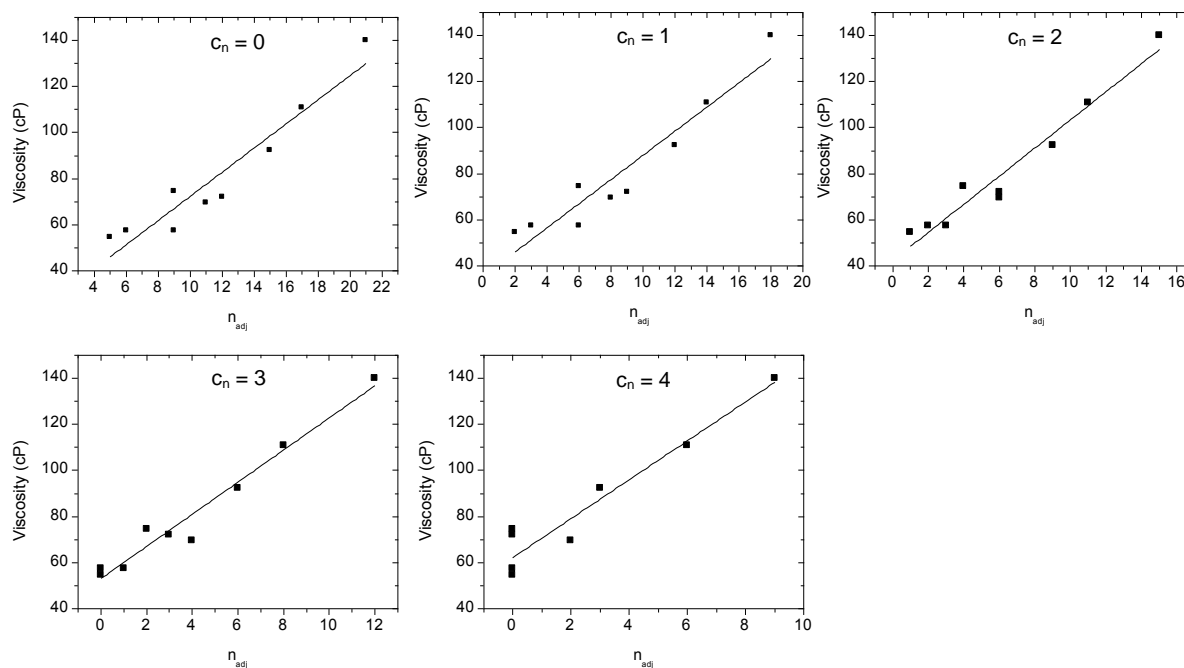


Figure 6. Plot of viscosity vs. n_{adj} for c_n values from 0 to 4, corresponding to a minimum alkyl chain length of methyl to propyl. Best fittings are found for c_n equal to 2 or 3; fittings with smaller c_n show a low slope region at low c_n , showing that $-\text{CH}_2-$ units close to the triazolium ring do not contribute much to viscosity. The plot for $c_n = 4$ shows a poorer R^2 value due to the exclusion of many $-\text{CH}_2-$ units that contribute to viscosity.

The maximum of R^2 is obtained for $c_n = 3$; the R^2 parameter for $c_n = 2$ is similar. These results are in reasonable agreement with the SAXS data of other alkyl-functionalized ILs, suggesting that very short alkyl chains in the trialkyltriazolium ILs are unable to participate in the formation of non-polar domains.

Substitution of a methyl-branched chain for an n -propyl group alkyl chain of the same overall number of carbon atoms resulted increased viscosity, compared to the corresponding n -alkyl substituted IL. The increase in viscosity was not linear with the number of branched alkyl chains, as can be seen by the much smaller increase in viscosity between $[\text{Tz}3\text{n}3\text{n}3\text{n}][\text{Tf}_2\text{N}](\mathbf{3})$ and $[\text{Tz}3\text{n}3\text{n}3\text{i}][\text{Tf}_2\text{N}](\mathbf{4})$ than between $[\text{Tz}3\text{n}3\text{n}3\text{i}][\text{Tf}_2\text{N}](\mathbf{4})$ and $[\text{Tz}3\text{i}3\text{i}3\text{i}][\text{Tf}_2\text{N}](\mathbf{5})$. The great

increase in viscosity observed for the [Tz3i3i3i][Tf₂N](**5**) and [Tz4i4i4i][Tf₂N](**9**) ILs may arise from multiple factors, which will be discussed in the following sections.

3.3.3 Self-Diffusion

The self-diffusion coefficients listed in Table 4 for the cation (D₊) and of the anion (D₋) ranged between 6.67E-12 and 3.72E-11; very similar to those observed at this temperature in dialkylimidazolium Tf₂N ILs.⁵⁸ Cation and anion diffusion values were both slightly greater for the triazolium ILs when compared on the basis of the total number of carbon atoms in the alkyl chains, probably due to both the increased viscosity caused by the longer maximum alkyl chain length in the imidazolium ILs and the decreased number of hydrogen bond donors on the triazolium ring. The “crossover point” at which the diffusion coefficient of the anion becomes greater than that of the cation occurs between $n=6$ and $n=9$, consistent with the imidazolium cation behavior.³³

3.3.4 Stokes-Einstein Analysis

The Stokes-Einstein relationship (Equation 11) relates the radius of a diffusing particle to its diffusion coefficient and the viscosity of the solution.⁴¹

$$D = \frac{kT}{c\pi\eta r} \quad (11)$$

Where D is the self-diffusion coefficient of the species, k is Boltzmann’s constant, T is the absolute temperature, η is the viscosity, and r is the hydrodynamic radius of the particle in

solution. The factor c is a coefficient describing the microscopic friction between the particle and the solvent; in classical hydrodynamic theory, it may take values between 4 and 6.

The Stokes-Einstein equation is based on the assumption of Stokes flow of the solution surrounding the diffusion particle; that is, that the particle experiences the solvent as continuous medium. While never physically the case for real solutions, this is the approximate situation for a particle that is much larger than the molecules of its solvent. However, the Stokes-Einstein equation has been reported to give accurate hydrodynamic radii even in situations far away from Stokes flow conditions, including the self-diffusion of neat substances, and even solutions in which the solute:solvent diameter ratio is as low as 0.5.⁶⁹

Due to instrumental limitations, acquisition of viscosity and diffusion coefficients at the same temperature for the trialkylimidazolium ILs was not possible, preventing application of the Stokes-Einstein equation to the data to calculate the hydrodynamic radii. However, by assuming that the temperature dependence of both properties is similar, the diffusion behavior of different ILs may be compared on a relative basis. The results should be interpreted with care, however, as many ILs show fragile and glassy dynamics; it is possible that some of the ILs may be close enough to their glass transition temperatures to exhibit non-Arrhenius temperature dependence of one or the other properties and thus violate this assumption.

Assuming a constant slip-stick parameter c , the diffusion behavior of the ions should thus be proportional to $D_{\pm} \propto 1/\eta r_{H\pm}$. Assuming a spherical radius, the hydrodynamic radius may be estimated from the calculated van der Waals volume of the cation as $r_H = \left(\frac{3}{4\pi} \frac{v_{vdW+}}{N_A}\right)^{\frac{-1}{3}}$. As shown in Figure 7, the relative dependence of the both the cation and anion diffusion coefficients is well described by the Stokes-Einstein equation. The hydrodynamic radii of the two smaller cations, [Tz3n11](**1**) and [Tz4n11](**2**), show a different dependence on viscosity than the rest of

the IL series. Such a difference could be explained by the limited interaction between the very short alkyl chains of these cations, as described in Section 3.3.2.

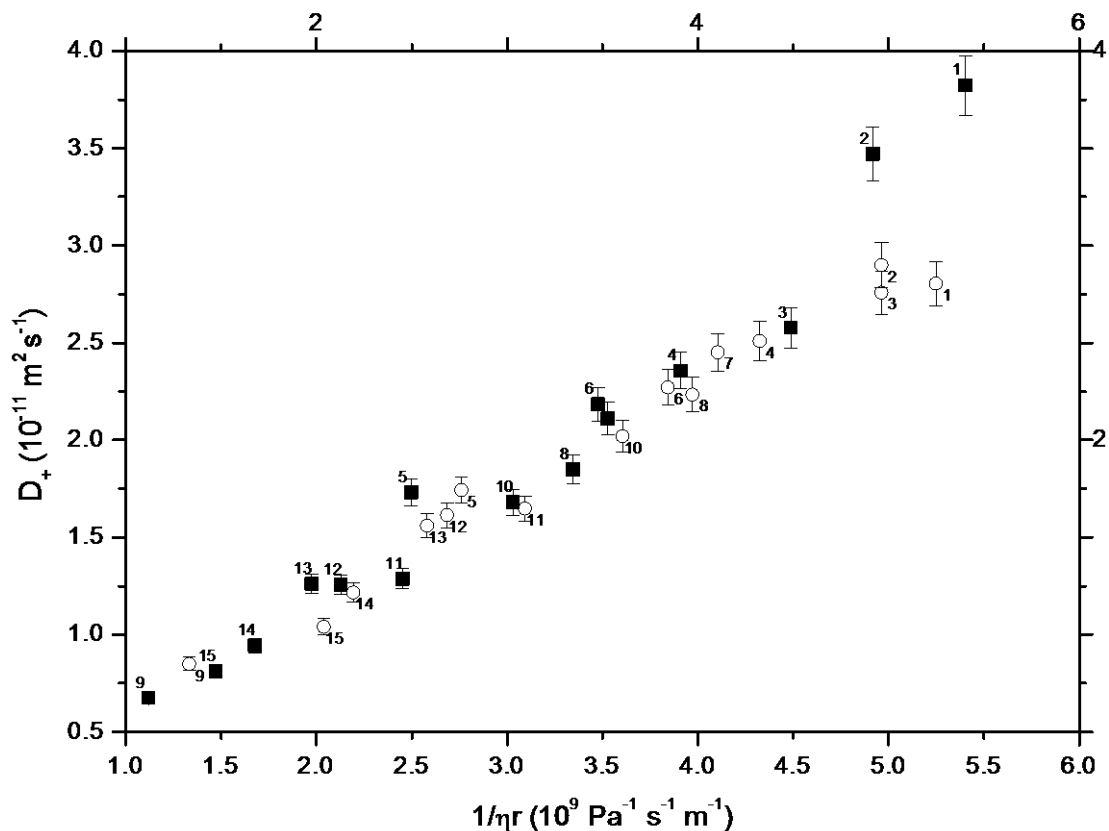


Figure 7. Self-diffusion coefficient D vs. $1/\eta r$. In the case of ideal hydrodynamic behavior, a linear relationship would be expected. Horizontal error bars are within the size of the points. Filled squares represent the cation; open circles represent the anion. Numbering of the ILs is given in Table 1.

Although the above analysis establishes the relationship between D and $1/\eta r$, due to the temperature discrepancy between the viscosity and diffusion data, it is not possible to know whether the hydrodynamic ionic radii are systematically larger or smaller than their computationally predicted values. However, the use of a common anion among all ILs allows this comparison. From equation 11, the ratio of the hydrodynamic radii of the ions will be the

inverse of the ratio of their diffusion coefficients, $\frac{r_{H+}}{r_{H-}} = \frac{D_+}{D_-}$; this ratio can then be compared with the computationally determined one. As shown in Figure 8 below, the experimental $\frac{r_{H+}}{r_{H-}}$ is always smaller than the calculated ratio. As the total number of $-\text{CH}_2-$ units rises from 5 to 12, the ratio of experimental:computational $\frac{r_{H+}}{r_{H-}}$ rises with a slope of about 2.2. This suggests that the increased alkyl-alkyl interactions at longer chain lengths slow the cation diffusion more than anion diffusion. The experimental (calculated from measured self-diffusion coefficients) r_{H+}/r_{H-} ratio plateaus at about 1.25 for n of 15 methylene units or greater. This effect has been observed previously in the dialkylimidazolium ILs, where it was attributed to greater interdigitation of the alkyl chains in the non-polar domains.^{33,53} Recent SAXS experiments have also suggested that at a total alkyl chain lengths of 13 $-\text{CH}_2-$ units or greater, the intensity of the SAXS peak corresponding to anion-anion ordering in the liquid plateaus at nearly zero; indicating that anions in such ILs have increased motional freedom and thus greater relative diffusion coefficients.³³

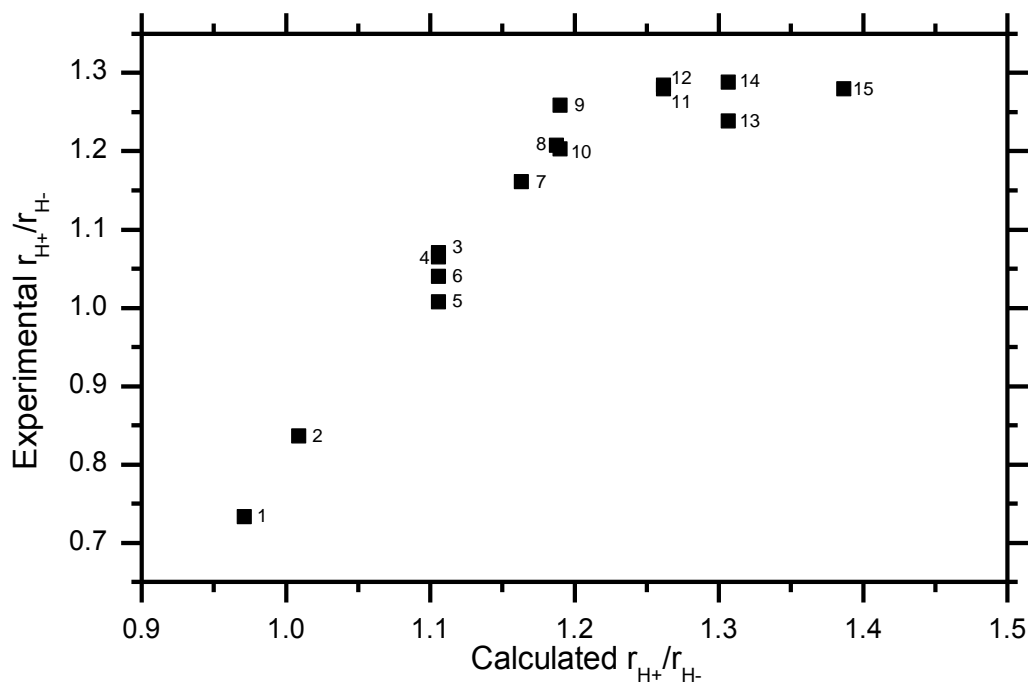


Figure 8. Experimental vs. calculated, r_{H^+}/r_{H^-} ratios of the ILs. Although the size of the cation increases along the whole IL series, a plateau is observed for ILs with MW > 560, suggesting that anion diffusion is limited by the diffusion of the cation in these ILs. Numbering of the ILs is given in Table 1.

The wide range of the plot in Figure 7 made difficult the comparison of the small variations of the viscosity-diffusion between isomeric cations. To better show the effect of isomerization on the self-diffusion of the ILs, data from the same experiments are presented in a slightly different format in Table 6 below. To provide a relative numerical value of hydrodynamic radius for each species, the values $1/\eta D_+$ and $1/\eta D_-$ are listed for each IL. Since the calculated ionic volumes were near identical for all isomeric cations, the relative hydrodynamic radius is not used as a normalization factor. The data in Table 6 should be treated with the same caveats that apply to comparing the viscosity and self-diffusion coefficients of the anion above.

Table 6. Comparison of Relative Hydrodynamic Radii of Isomeric ILs.

n	IL	Cation	$D_+ / 10^{-11}$ $m^2 s^{-1}$	$D_- / 10^{-11}$ $m^2 s^{-1}$	D_+/D_-	$1/\eta D_+$ $/10^8 s P^{-1}$ m^{-2}	$1/\eta D_-$ $/10^8 s P^{-1}$ m^{-2}
9	3	Tz3n3n3n	2.56	2.78	0.92	6.78	6.25
	4	Tz3n3n3i	2.35	2.50	0.94	6.44	6.05
	5	Tz3i3i3i	1.74	1.74	1.00	5.55	5.55
	6	Tz4n14n	2.16	2.21	0.98	6.22	6.08
12	8	Tz4n4n4n	1.85	2.22	0.83	7.51	6.26
	9	Tz4i4i4i	0.67	0.82	0.78	6.99	5.69
	10	Tz8i3n1	1.68	2.02	0.83	7.51	6.24
15	11	Tz5n5n5n	1.34	1.69	0.79	8.08	6.40
	12	Tz7i7n1	1.25	1.59	0.79	7.52	5.91
17	13	Tz7n7n3n	1.26	1.56	0.81	7.16	5.79
	14	Tz8i8n1	0.99	1.27	0.78	7.78	6.06

On the basis of their lower $1/\eta D$ values for both cation and anion, ILs containing the cations with three branched alkyl chains, [Tz3i3i3i][Tf₂N](**5**) and [Tz4i4i4i][Tf₂N](**9**) seem to experience abnormally fast diffusion relative to their viscosity. This observation is unexpected, given that the calculated van der Waals volumes of [Tz3i3i3i][Tf₂N](**5**) and [Tz4i4i4i][Tf₂N](**9**) are equal to those of their isomers. In the absence of data regarding the melting temperatures and crystallization or glass transition temperatures, the possibility that the anomalously fast diffusion is due to the onset of vitrification in these ILs cannot be ruled out. However, their faster diffusion is also consistent with the greater ionicity ratios observed for these ILs (see Section 3.3.7). A greater fraction of the diffusive motions in the triply-branched ILs occur as single-ion displacements rather than as correlated displacements of an anion and cation, compared to their isomers. The diffusion coefficient of the single ion transport process would be expected to be greater relative to viscosity than that of a correlated cation-anion displacement, which could explain the greater relative values of these ILs.

The IL [Tz7i7n1][Tf₂N] (**15**) shows faster diffusion relative to viscosity than [Tz5n5n5n][Tf₂N](**11**); however, [Tz8i8n1][Tf₂N](**14**) shows slower diffusion than [Tz7n7n3n][Tf₂N](**13**), perhaps because of its greater ionicity ratio. The relationship between hydrodynamic radius, ionicity, and diffusion coefficient is thus less clear for relatively long total alkyl chain length.

3.3.5 Ionic and Molar Conductivities

The ionic conductivities are listed in Table 4 above for the trialkyltriazolium Tf₂N ILs. The ionic conductivities ranged from 0.03 to 0.52 S m⁻¹: a similar range to that observed in dialkylimidazolium Tf₂N ILs.^{33,58} The conductivity values were slightly greater for the triazolium ILs when compared on the basis of the number of carbon atoms in the alkyl chains, as with diffusion; this may be due to both the increased viscosity caused by the longer maximum alkyl chain length in the imidazolium ILs and the decreased number of hydrogen bond donors on the triazolium ring.

3.3.6 Walden Plot Analysis

The Walden relationship, an empirically-derived relationship between the ionic conductivity and solvent viscosity for dilute electrolyte solutions, states that the limiting molar conductivity Λ_0 of an infinitely dilute electrolyte solution will be related to the viscosity of the solvent by the relationship⁴⁹

$$\Lambda_0 \eta = C \quad (12)$$

where C is an electrolyte-specific constant. This relationship has been used to analyze the deviation of electrolyte solutions from ideality through the so-called Walden Plot, an analysis method that is based on the fact that in ideal, fully dissociating electrolyte solutions such as aqueous 0.01M KCl, the plot of $\log(\Lambda)$ vs. $\log(1/\eta)$ yields a line of slope one and an intercept of 0. The negative deviations of $\log(\Lambda)$ from the KCl line give the degree of non-ideality of the solution.^{70,71}

As viscosity and conductivity data could not be obtained at the same temperature due to instrumental limitations, a comparison of the data to an ideal electrolyte line such as the KCl line could not be performed. However, a measure of the relative deviations among the ILs from ideal Walden behavior can be obtained through the assumption used in the Stokes-Einstein analysis above, that is, that the viscosities of the ILs at 22 °C are proportional to their 30 °C values. A plot of the values of molar conductivity vs. $1/\eta$ appears in Figure 9 below. The caution that the ILs may show glassy dynamics and non-Arrhenius temperature dependence of their transport properties also applies to this analysis.

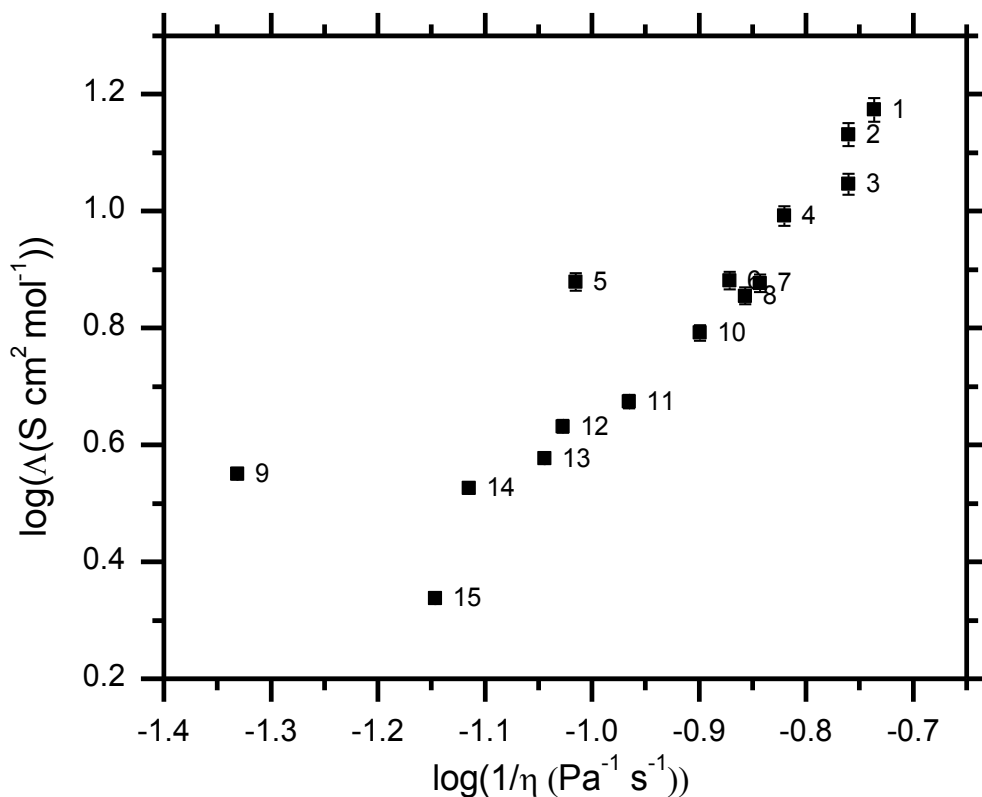


Figure 9. Walden-type plot of conductivity and viscosity data. In the absence of correlated cation-anion motions, a linear relationship would be expected. The conductivities of [Tz3i3i3i][Tf₂N] and [Tz4i4i4i][Tf₂N] are aberrantly high compared to those of the *n*-alkyl and singly-branched ILs. Horizontal error bars are within the point size. Numbering of the ILs is given in Table 1.

The plot shows a near-linear dependence of the log of conductivity on the log of inverse viscosity. The two large outliers in the positive direction are the tri-branched ILs [Tz3i3i3i][Tf₂N](**5**) and [Tz4i4i4i][Tf₂N](**9**); similar to the observation made of their self-diffusion coefficients, the conductivity of these ILs is larger than would be expected for an *n*-alkyl IL of the same viscosity. In the absence of data regarding the melting temperatures and glass transition temperatures, if these ILs prove to be glass formers, the possibility that the anomalously fast diffusion is due to the onset of vitrification in these ILs cannot be ruled out. However, their faster diffusion is also consistent with the greater ionicity ratios observed for

these ILs (see Section 3.3.7). The large outlier in the negative direction is [Tz7n7n7n][Tf₂N](**15**); as this IL was not noted to have an unusual relationship between diffusion and viscosity, or in the ratio of its ions' diffusion coefficient, the origin of this behavior is not clear.

3.3.7 Nernst-Einstein Deviation

As discussed in the introduction, the ionicity ratio is a measure of the correlation between the motion of cations and anions. Ions may diffuse singly, thus contributing to both conduction and diffusion; or simultaneously with an oppositely charged counterion, thus contributing to diffusion but not conductivity. The relative frequency of each type of movement will be determined by the balance of forces between the energy needed to form a hole large enough to accommodate either a single ion or ion pair, and the energy needed to break the specific interactions of an ion or ion pair with their neighboring ions.

The Nernst-Einstein deviation parameter $\frac{\Lambda_{imp}}{\Lambda_{NMR}}$, or ionicity, was calculated for the trialkyltriazolium Tf₂N ILs. As has been found for the 1,3-dialkylimidazolium cation^{55,58} the ionicity decreased with increasing alkyl chain length. The ionicity ratios of the tri-branched ILs [Tz3i3i3i][Tf₂N](**5**) and [Tz4i4i4i][Tf₂N](**9**) were larger than those of their *n*-alkyl analogues; with the increase in ionicity ratio for [Tz4i4i4i][Tf₂N](**9**) being much larger than for [Tz3i3i3i][Tf₂N](**5**) (29% vs. 7%). It is clear that the increased branching causes a great increase in viscosity, and decrease in diffusion and conductivity for these ILs. However, the self-diffusion and conductivity processes are faster than would be estimated for their ILs of their viscosity, based on the viscosity-transport correlations of the *n*-alkyl and singly-branched ILs. This would seem to indicate that the changes to the solution structure of these ILs caused by the increased

branching arrest paired-motions to a greater extent than single motions. As was discussed previously, in the absence of data regarding the glass transition temperatures of these ILs, if indeed they prove to be glass formers, glassy dynamics cannot be ruled out as origin of the anomalous ionicity ratios. However, if this does not prove to be the case, several other possible explanations can be advanced. The reduction in paired motion can be justified on the basis of either the greater steric hindrance produced by the presence of branching near the triazolium core weakening the specific cation-anion chemical interactions, or the differing distribution of free volume within the IL decreasing the possibility of the formation of holes large enough for a concerted cation-anion jump.

The cavity model of diffusion for ILs suggests that ionicity should be correlated to the free molar volume within the liquid. A plot of ionicity against free molar volume is shown in Figure 10 below. The data appear to be clustered into two approximately linear, but discontinuous groups. The common feature within each group appears to be the length of the longest alkyl chain. The group marked by the upper curve contains all ILs whose longest alkyl chain has less than four $-\text{CH}_2-$ units, as well as $[\text{Tz4n11}][\text{Tf}_2\text{N}](2)$. The basis for the discontinuity may be explained on the basis of alkyl-alkyl interactions within the IL. The butyl chain length has been previously identified by SAXS measurements as the minimum chain length at which inter-cation alkyl-alkyl correlations begin to form within an IL; linear regression analysis of chain length for the n -alkyl substituted anions in this study confirmed that α and β $-\text{CH}_2-$ groups make little contribution to the viscosity of the IL. On this basis, it would seem that the discontinuity of the two approximately linear regions indicates that a change in the balance of interactions that determine the balance of single ion diffusion and ion pair diffusion occurs upon the organization of the liquid into polar and non-polar domains. The exceedingly high ionicity of

the IL [Tz4i4i4i][Tf₂N](**9**), however, is not explained as it has a free volume similar to that of its *n*-alkyl analogue, [Tz4n4n4n][Tf₂N](**8**); evidently there is some anomaly in the structure of this IL that favors single ion diffusion mechanism that cannot be explained by free volume considerations alone. The presence of the non-polar domains should favor the diffusion of ion pairs, from a free volume perspective, as the non-polar domains consist of flexible alkyl chains that associate with each other on the basis of the weaker van der Waals forces.

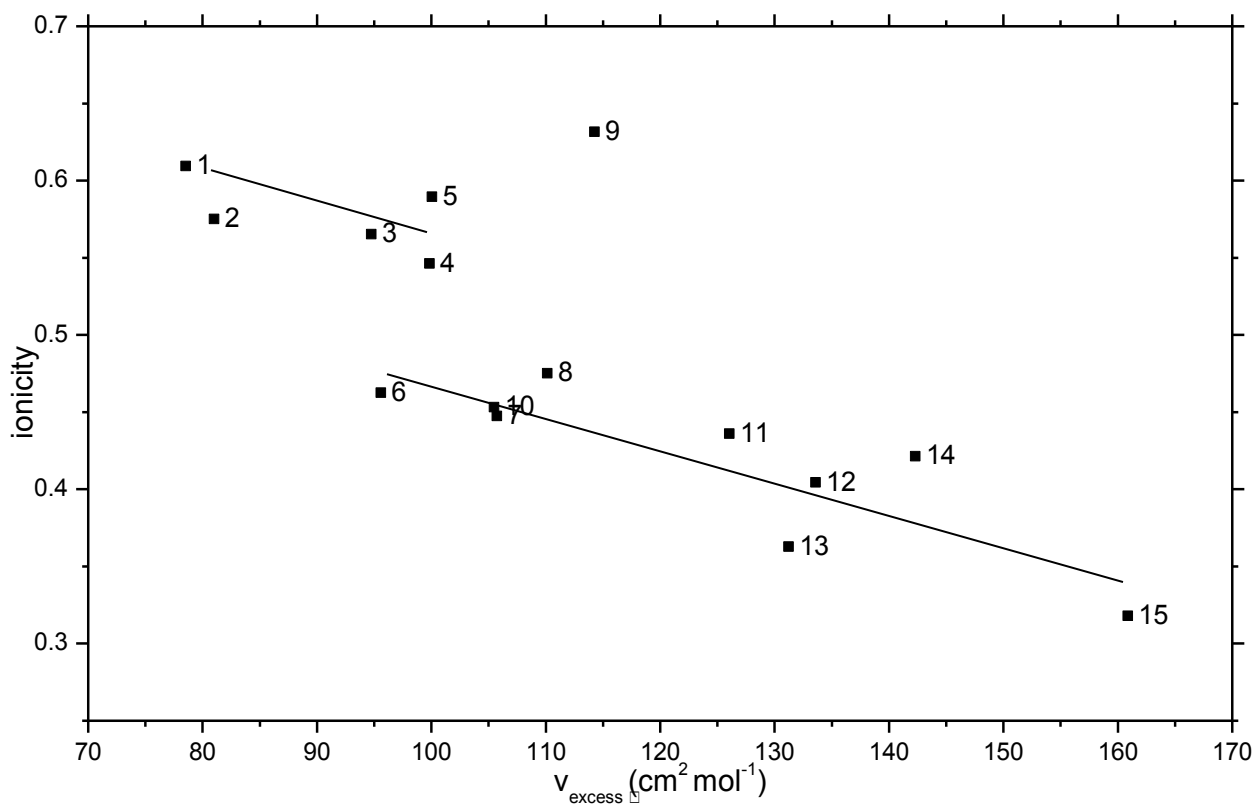


Figure 10. Ionicity ratio vs. excess molar volume. Lines are included as guides to the eye only. Numbering of the ILs is given in Table 1.

The great decrease in transport properties for the tri-branched ILs may then indicate that because their branched alkyl chains are effectively one $-\text{CH}_2-$ unit shorter than the number of $-\text{CH}_2-$

CH₂⁻ units they contain, and they thus behave as ILs with little or no formation of non-polar domains. Compared to the smaller cations such as [Tz3n11](**1**) and [Tz4n11](**2**), the tri-branched cations are bulkier and more rigid, but no increase in flexible space within the liquid compensates this bulk. Both paired and single diffusion of the ions will therefore be more unfavorable, but paired diffusion especially so. A similar effect has been proposed to explain the transport behavior of the ILs with the 1-methyl-3-butylimidazolium and 1,2-dimethylbutylimidazolium cations; upon substitution of a methyl group for the hydrogen the transport properties of the liquid decrease greatly.⁷² In fact, a measurement of the ionicity ratios for 1-methyl-3-butylimidazolium tetrafluoroborate and 1,2-dimethyl-3-butyl tetrafluoroborate also showed an increase in the ionicity ratio from .61 to .79; however, the purity of the latter sample was suspect.⁷³

3.4 NMR CHEMICAL SHIFT DATA

The 1D ¹H and ¹⁹F proton spectra were recorded for all of the ILs; experimental details, as well as peak data and assignments appear in the experimental section.

The origins of the variations in chemical shift among ILs of the same family are complex, arising from both on both inter-ionic and intra-ionic effects. The trialkyltriazolium Tf₂N ILs contain several moieties known to affect the chemical shifts of nearby nuclei due to their magnetic anisotropy; namely, the aromatic ring and sulfone groups create a strong shielding cones above the ring plane and a deshielding cones along the axis of the S=O bond.⁷⁴ Additionally, the cation and anion contain several potential hydrogen bond donor and acceptor atoms, respectively.

A previous study on the ^{19}F chemical shift of the Tf_2N anion found that for a given cation family, the ^{19}F chemical shift moved downfield with increasing molar volume; the decrease in δ was well-correlated with the average interionic distance, estimated as the inverse cube root of molar volume, and relatively insensitive to the addition of $-\text{OH}$ groups to the alkyl groups of the cation.⁷⁵ The authors attributed these findings to the dependence of the chemical shift on the local electrostatic environment; with the density of Coulomb charges assumed to decrease as interionic distance increased. As shown in Figure 11, the same dependence is observed in the n -alkyl and singly-branched trialkyltriazolium Tf_2N ILs.

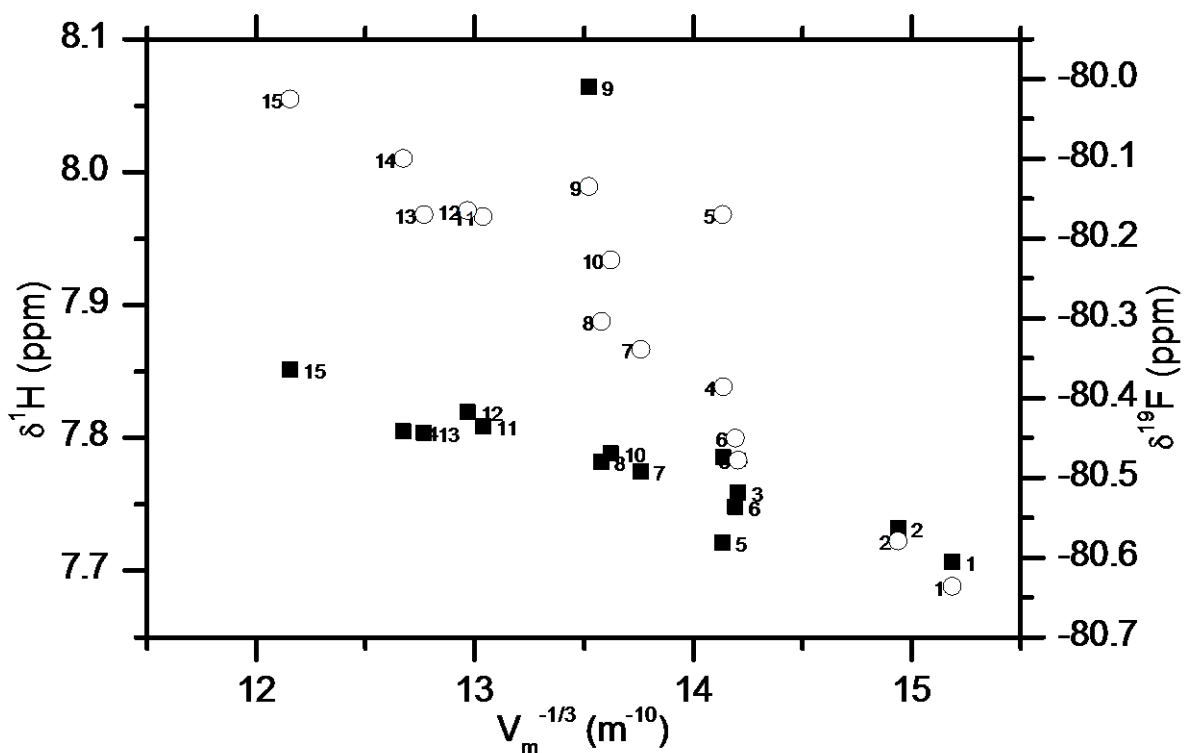


Figure 11. ^1H shift of proton H5 and ^{19}F Chemical Shift of $-\text{CF}_3$ vs. $(v_m)^{1/3}$ Filled squares represent the cation; open circles represent the anion. Numbering of the ILs is given in Table 1.

A similar dependence is observed for the H5 protons of the triazolium ring, as well as for the CH₂ protons α to the triazolium ring (see experimental section). The behavior of the chemical shifts of the [Tz3i3i3i][Tf₂N](**5**) and [Tz4i4i4i][Tf₂N](**9**) cations thus seems to indicate greatly altered electrical environments in these ILs. The [Tz4i4i4i][Tf₂N](**9**) IL exhibits both a strongly downfield H5 signal and a slightly downfield shifted ¹⁹F signal relative to its molar volume, while [Tz3i3i3i][Tf₂N](**5**) shows only a deshielded ¹⁹F signal. Such altered magnetic environments in these ionic liquids may be further evidence of a differing liquid structure within these ILs.

3.5 CARBON DIOXIDE SOLUBILITY DATA

3.5.1 Results

CO₂ solubility data were provided by Dr. Eric Albenze at the NETL Laboratory in Pittsburgh, PA. Details of the experimental setup and conditions used for the gas solubility measurements can be found in the Experimental Section.

The solubility of a gas in an IL is conventionally reported as the value of the coefficient of Henry's Law,

$$p=k_Hx \quad (13)$$

where p is the partial pressure of the gas above the liquid, x is the mole fraction of the gas dissolved in the liquid, and k_H is the empirically determined constant for a gas/solvent pair at a given temperature. The Henry's Law constants for the ILs studied are listed in Table 7 below.

Table 7. Henry's Law Constants of Carbon Dioxide Solubility for the ILs Studied.

IL	Cation	K_H / bar^a
1	Tz3n11	32.0
2	Tz4n11	30.0
3	Tz3n3n3n	27.7
4	Tz3n3n3i	27.6
5	Tz3i3i3i	32.2
6	Tz4n14n	27.9
7	Tz5n5n1	26.7
8	Tz4n4n4n	27.8
9	Tz4i4i4i	27.8
10	Tz8i3n1	25.2
11	Tz5n5n5n	25.2
12	Tz7i7n1	23.6
13	Tz7n7n3n	23.6
14	Tz8i8n1	21.7
15	Tz7n7n7n	21.0

^a Henry's Law constant data provided by Dr. Eric Albenze. Error of the measurement was ± 1.5 bar.

3.5.2 Statistical Correlation with Physical and Transport Parameters

One of the principal aims of the collaborative project described in this thesis was to study the possible relationship of the ionicity parameter of an IL with its ability to solvate CO₂. As described in the introduction, the predictive variable of greatest usefulness thus far has been the molar volume of the IL. At the outset of the project, it was hypothesized that given the great effect of the anion on carbon dioxide solubility in ILs, increased ionicity might have some favorable effect on the solubility of carbon dioxide by lowering the strength cation-anion interactions, making the anion more chemically available for favorable IL-gas interactions. Since then it has become clear both from the results reported in this thesis, as well as from reviews of literature data, the increased ionicity ratios are in fact negatively correlated with the solubility of CO₂.

However, given the relationship proposed between ionicity and the transport properties of the ions within the IL, it then seemed reasonable to investigate the possible relationship of carbon dioxide solubility to ionicity, as well as the other physical parameters that have been identified as having possible correlations to the carbon dioxide solubility, such as free volume. The solubility of carbon dioxide is likely to be determined by a number of interacting factors, which will themselves be correlated. To understand the relative predictive value of each of the parameters, single- and multivariate linear regressions were carried out, and the statistical significance of each parameter was evaluated by t-test. The adjusted R^2 values and the p-value parameter of the t-test for statistical significance are reported in Table 8 below.

Table 8. Statistical Significance of Molar Volume and Ionicity Parameters for K_H Determination.

<i>K_H vs. Molar Volume</i>	
Adjusted R^2 : 82.0%	
Parameter	p-value
Molar Volume	<0.001
<i>K_H vs. Ionicity</i>	
Adjusted R^2 : 72.5%	
Parameter	p-value
Ionicity	<0.001
<i>K_H vs. v_{excess}</i>	
Adjusted R^2 : 80.5%	
Parameter	p-value
v_{excess}	<0.001
<i>K_H vs. Molar Volume, Ionicity</i>	
Adjusted R^2 : 85.0%	
Parameter	p-value
Overall Correlation	<0.001
Molar Volume	0.005
Ionicity	0.084
<i>K_H vs. v_{excess}, Ionicity</i>	
Adjusted R^2 : 86.5%	
Parameter	p-value
Overall Correlation	<0.001
v_{excess}	0.003
Ionicity	0.023

Among single parameters, molar volume was the best predictor of K_H , with an R^2 value of 82.0%; the parameters v_{excess} and ionicity performed slightly worse. The addition of ionicity as a second predictor to molar volume or v_{excess} improved the R^2 ; however, in the case of molar volume the p-value of ionicity was larger than the .05 cutoff usually used as the maximum threshold of statistical significance. For the regression of ionicity and v_{excess} with K_H , the p-value for ionicity was improved, to 0.023. However, due to the small sample size and high degree of correlation between ionicity and v_{excess} , it is unclear whether this correlation represents a relationship with an underlying physical significance. The correlation with the greatest overall fit was K_H vs. v_{excess} and ionicity; however the improvement to the R^2 value should also be

interpreted with caution due to the correlations of the predictors to each other; the addition of a second predictive variable often improves R^2 due to correlations between the predictive variables. Thus, conclusive statistical evidence for an independent effect of the ionicity ratio on the solubility of CO_2 in a given IL.

3.5.3 Effect of Isomerization

The IL $[\text{Tz3i3i3i}][\text{Tf}_2\text{N}](\mathbf{5})$ displayed the poorest carbon dioxide of all of the trialkyltriazolium ILs measured. Interestingly, although $[\text{Tz4i4i4i}][\text{Tf}_2\text{N}](\mathbf{9})$ shows greater deviation in its transport and spectroscopic properties, its Henry's Law constant is equal to that of its *n*-alkyl isomer $[\text{Tz4n4n4n}][\text{Tf}_2\text{N}](\mathbf{8})$. The poor solubility of CO_2 in $[\text{Tz3i3i3i}][\text{Tf}_2\text{N}](\mathbf{5})$ compared to its isomers is also unexpected, as the molar volume and v_{excess} of $[\text{Tz3i3i3i}][\text{Tf}_2\text{N}](\mathbf{5})$ is greater than that of its isomers. However, the rigidity and bulk of the isopropyl groups may give rise to many fewer cavities within the liquid that are large enough to accommodate a CO_2 molecule. In contrast, the more flexible 1-methylpropyl moiety at the terminal end of two of the alkyl chains of the $[\text{Tz4i4i4i}](\mathbf{9})$ cation will have greater conformational freedom, and thus easily form cavities large enough to accommodate CO_2 , while still having a small amount of cavities large enough to accommodate ion diffusion.

4.0 CONCLUSIONS

The effect of cation structure on molar volume, viscosity, self-diffusion coefficients, and conductivity were evaluated for 15 novel ILs from the 1,2,4-trialkyl-1,2,3-triazolium Tf₂N IL family. The densities and transport properties of the straight chain alkyl *n*-alkyl chain were found to be similar to those of the well-studied 1,3-dialkylimidazolium Tf₂N family, and followed the same trends as the imidazolium family, when compared on the basis of the sum of the alkyl chain lengths.

The inclusion of multiple branched alkyl chains was found to have a dramatic impact on the transport properties while having minimal impact on the molar volume, thus providing another method of tuning the properties of ILs. The diffusion and conductivity of the ILs [Tz3i3i3i][Tf₂N](**5**) and [Tz4i4i4i][Tf₂N](**9**) showed anomalously high diffusion coefficients and molar conductivity values on the basis of the viscosity-diffusion and viscosity-conductivity relationships observed among the other ILs studied, as well as markedly increased ionicity ratios compared to those of their isomeric ILs. Two possible rationalizations for this behavior, glassy dynamics within these liquids, and/or decreased average cavity size within these ILs even at temperatures far from their melting or glass transition temperatures, were proposed. The ionicity ratio was found to decrease with increasing excess molar volume within the ILs. The dependence was found to be different for ILs with at least two *n*-alkyl chains of butyl length or longer; such a

difference was attributed to formation of non-polar domains being favorable for correlated cation-anion diffusion.

Henry's law constants for carbon dioxide solubility were determined for the ILs. No evidence to support the hypothesis that increased ionicity ratios enhance carbon dioxide solubility through increased activity of the anion was found. The IL [Tz3i3i3i][Tf₂N] displayed extremely poor carbon dioxide solubility compared to its isomers.

5.0 EXPERIMENTAL

5.1 GENERAL

ILs were synthesized by Dr. Michael Lartey at the NETL laboratories in Pittsburgh, PA. To avoid contamination of the sample by atmospheric water vapor, all sample transfers took place in a home-built dry box purged with a constant flow of dried air. The IL samples were stored in a vacuum desiccator when not in use.

Statistical analyses were carried out using the linear regression and multiple linear regression functions of Minitab 16.2.3 (Minitab Inc., State College, PA, USA).

5.2 DENSITY AND VISCOSITY MEASUREMENTS

Density and viscosity measurements were carried out by Dr. Michael Lartey at the NETL laboratories in Pittsburgh, PA

Density of ILs were measured at ambient temperature of 22 °C on a Micromeritic Accupyc II 1340 pycnometer (Micromeretic Instrument Corporation, Norcross, GA, USA) under constant flow of helium. All density measurements were performed in triplicate and the average recorded.

Viscosity measurements were carried out at ambient temperature of 22 °C on a Rheosense μ Visc (Rheosense Inc., San Ramon, CA, USA).

5.3 CARBON DIOXIDE SOLUBILITY MEASUREMENTS

Carbon dioxide solubilities were measured by Dr. Erik Albenze at NETL Pittsburgh. All solubility measurements were performed using a PCT-Pro2000 apparatus from Setaram Inc. The PCT-Pro 2000 is a Sievert's apparatus, which determines gas solubility in a sample by charging a leak-tight sample chamber of known volume with a known quantity of CO₂. The CO₂-charged sample chamber is isolated from the rest of the system and the pressure drop in the chamber is measured. The drop in pressure due to CO₂ absorption into the liquid is then measured, and the quantity of CO₂ absorbed into the liquid is easily determined from an equation of state, in this case, the NIST Standard Reference Database 23. For all tests, between 0.9 g and 1.5 g of the sample was loaded into the sample chamber. The sample was held under a dynamic vacuum for 4 hours prior to starting a test. During this evacuation, the sample was heated to 30 °C and was stirred at 300 rpm. After evacuation, testing was initiated by dosing the sample chamber with a known amount of CO₂, and the sample was allowed to equilibrate for at least 4 hours. Dosing was repeated to obtain an isotherm over a pressure range of 0–10 bar. Throughout all tests, the sample was held at 30 °C and was stirred at 300 rpm.

5.4 MOLAR VAN DER WAALS VOLUME COMPUTATIONS

The computations of the molar van der Waals volumes were carried out by Dr. James Mao at the University of Pittsburgh. Initial geometry optimization was performed using molecular force field optimization in the Avogadro software suite. Refinement of the geometry optimization and volume calculations were carried out using Gaussian, using the basis set B3LYP at the 6-31G* level of theory. Volumes were calculated using 100 points at the 0.002 electron density isosurface level.

5.5 NMR EXPERIMENTS

5.5.1 Experimental Details

NMR spectra were acquired using a Bruker Avance III spectrometer with a Bruker UltraShield magnet operating at a ^1H frequency of 600.71MHz, equipped with a Bruker BBFO Plus probe.

Samples were loaded into 3mm outer diameter NMR tubes to limit the effect of thermal convection on diffusion measurements. To provide a deuterium signal for the deuterium lock, as well as to provide a reference for accurate chemical shift determination, the 3mm NMR tubes were inserted coaxially into medium-walled NMR tubes with a sufficient amount of DMSO-d₆ in the outer tube to reach the height of the sample in the inner tube when inserted. Shimming was performed using the TOPSHIM gradient shimming macro incorporated in the Bruker TopSpin software suite, using a ^1H shimming routine with the excitation frequency set to a resonance originating from the IL. The spectrometer was tuned and matched before each experiment, and

the 90° pulse widths for the ^1H and ^{19}F spectra were determined using the nutation method via the built-in pulsecal macro.

Temperature was controlled at $30\text{ }^\circ\text{C} \pm 0.1\text{ }^\circ\text{C}$ via the spectrometer variable temperature unit and the probe thermocouple, with a constant gas flow of 670 l/h. Each sample was thermally equilibrated for at least 30 minutes prior to the start of acquisition. The thermocouple was calibrated using the known temperature dependence of the difference of OH and CH_3 resonances chemical shift of a sample of 80% ethylene glycol in DMSO-d₆.

PGF-NMR spectra for self-diffusion coefficient determination were recorded using the Bruker pulse sequence stebppg1s, which incorporates a stimulated echo, bipolar gradient pulse, and one spoil gradient. The value of diffusion time δ was 1 s and the total gradient pulse width Δ was 5 ms. Eight spectra, with gradient strength ramped linearly from 2% to 95% of the maximum gradient strength, were acquired with eight transients each, to produce a pseudo-2D diffusion spectrum. The decays of all observed peaks were fitted to a modified Stejskal-Tanner equation, incorporating the appropriate correction factors for the bipolar pulses, spoil gradients, and gradient shape, using the built-in relaxation analysis module in the Bruker TopSpin software suite.

5.5.2 Representative ^1H and ^{19}F Spectra and Fits of Diffusion Data to Stejskal-Tanner Equation

Typical fittings for four ILs appear below; the red line represents the Stejskal-Tanner equation for the diffusion coefficient calculated, and the open circles represent the observed intensity.

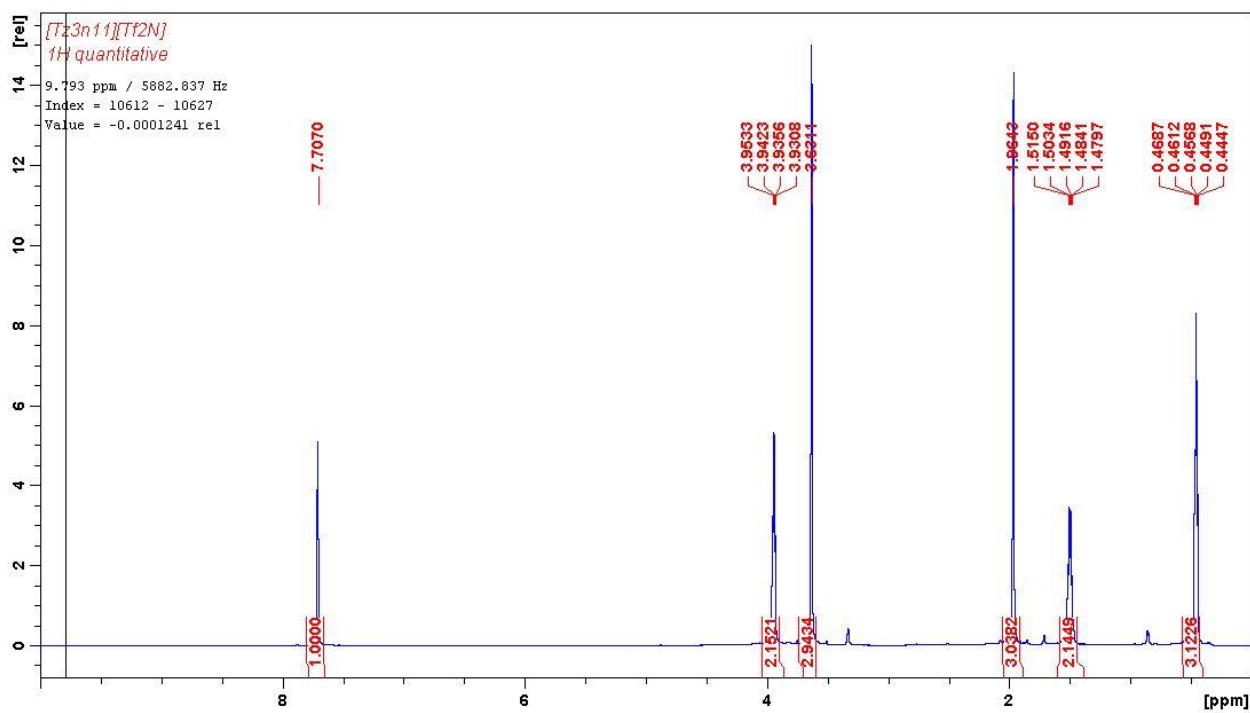


Figure 12. 1H NMR spectrum of $[Tz3n11][Tf_2N]$.

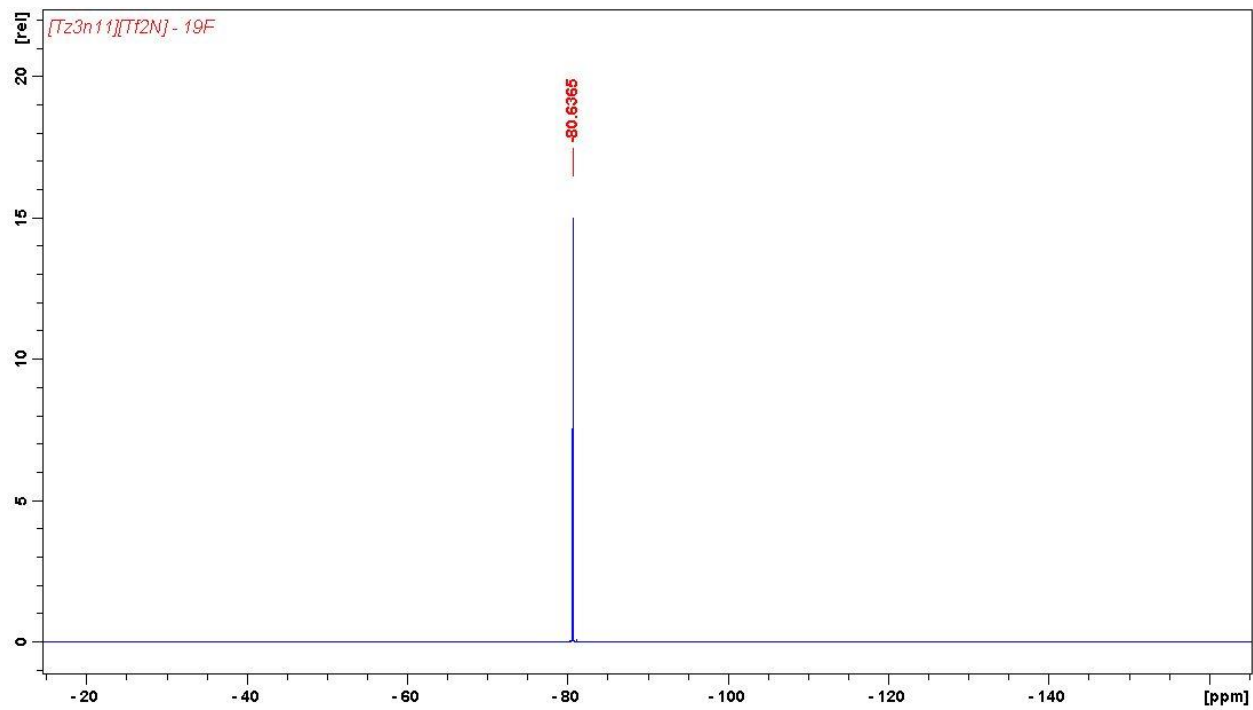


Figure 13. ^{19}F NMR spectrum of $[Tz3n11][Tf_2N]$.

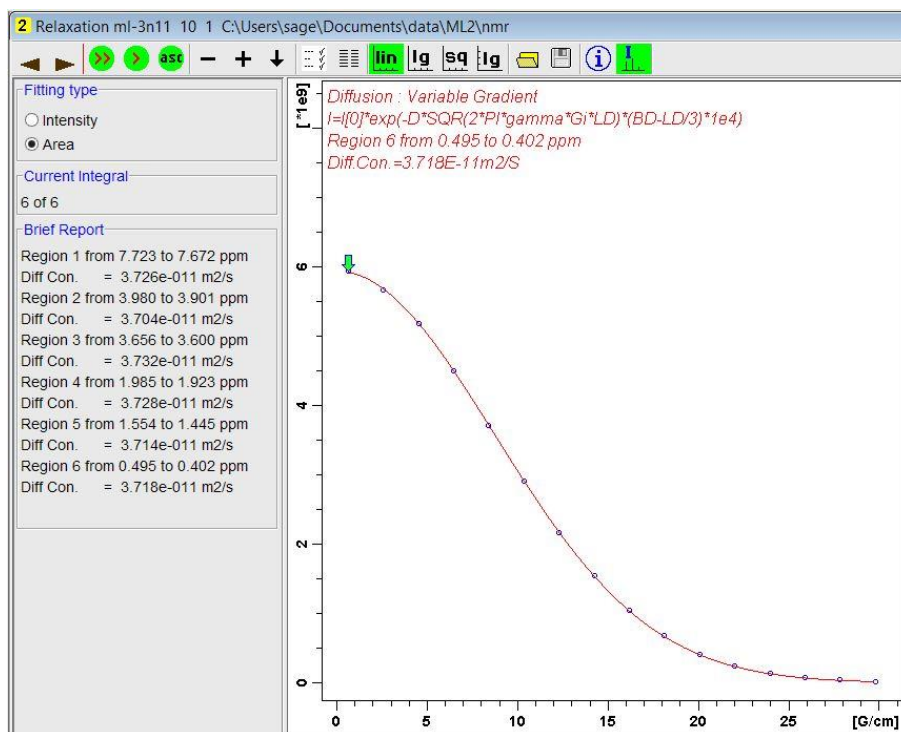


Figure 14. Fit of ^1H (cation) diffusion data to Stejskal-Tanner equation for $[\text{Tz3n11}][\text{Tf}_2\text{N}]$.

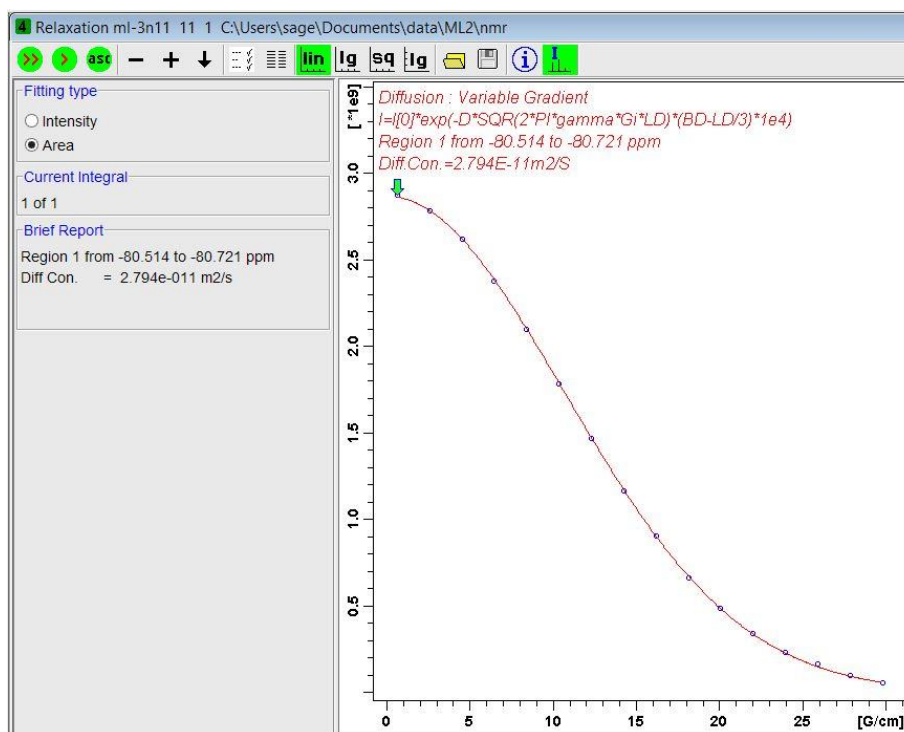


Figure 15. Fit of ^{19}F (anion) diffusion data to Stejskal-Tanner equation for $[\text{Tz3n11}][\text{Tf}_2\text{N}]$.

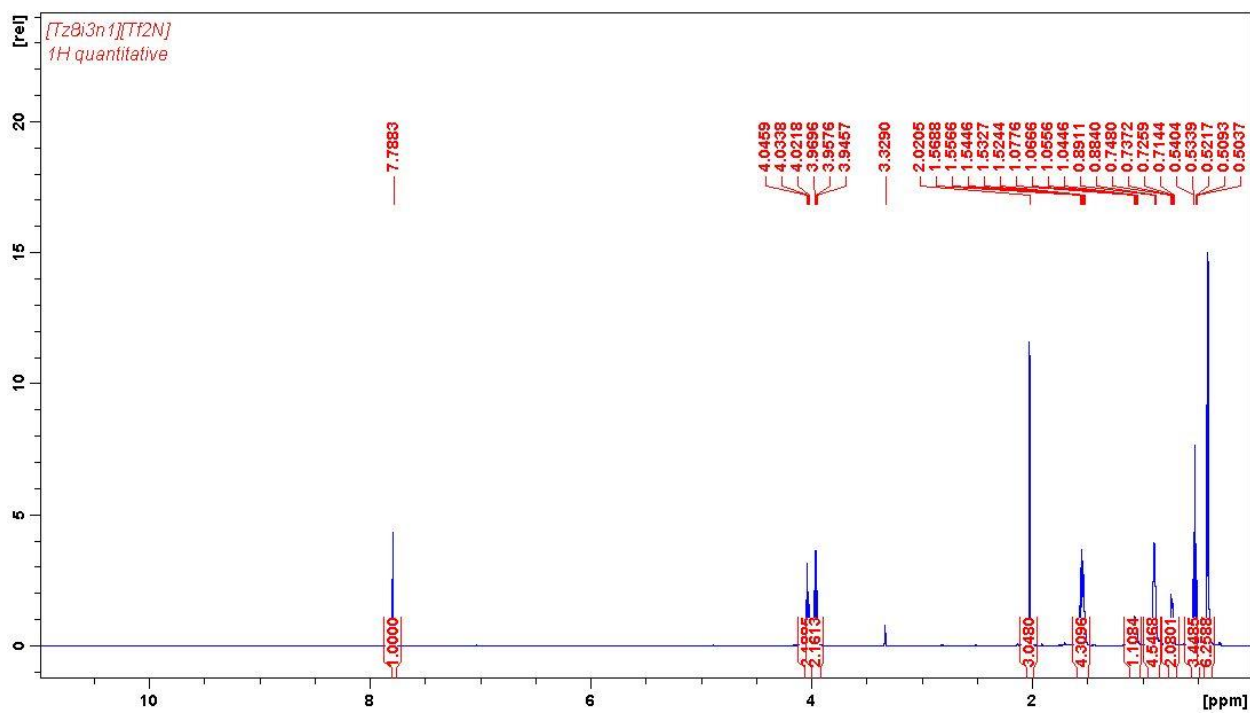


Figure 16. ^1H NMR spectrum of $[\text{Tz}8\text{i}3\text{n}1][\text{Tf}_2\text{N}]$.

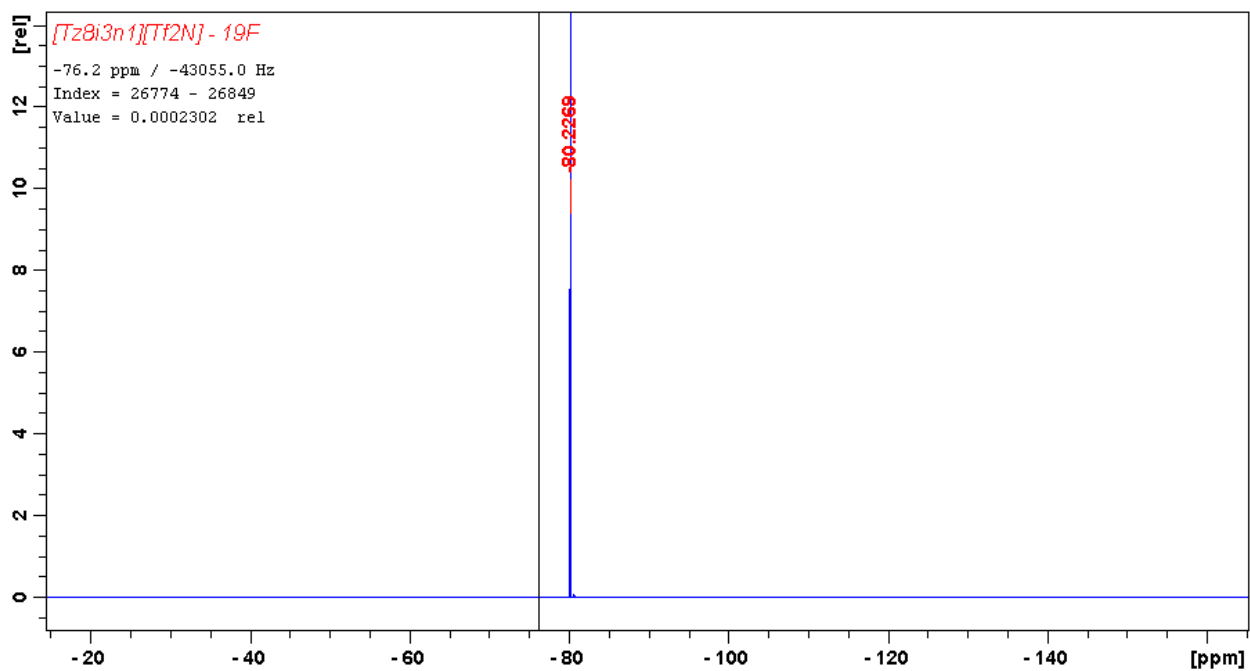


Figure 17. ^{19}F NMR spectrum of $[\text{Tz}8\text{i}3\text{n}1][\text{Tf}_2\text{N}]$.

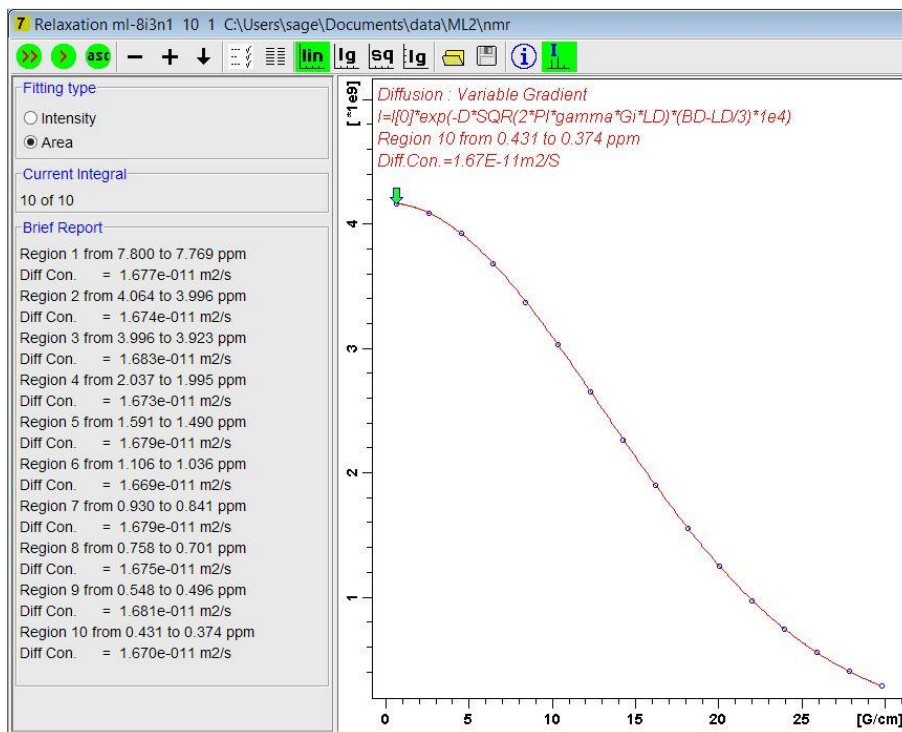


Figure 18. Fit of ^1H (cation) diffusion data to Stejskal-Tanner equation for $[\text{Tz8i3n1}][\text{Tf}_2\text{N}]$.

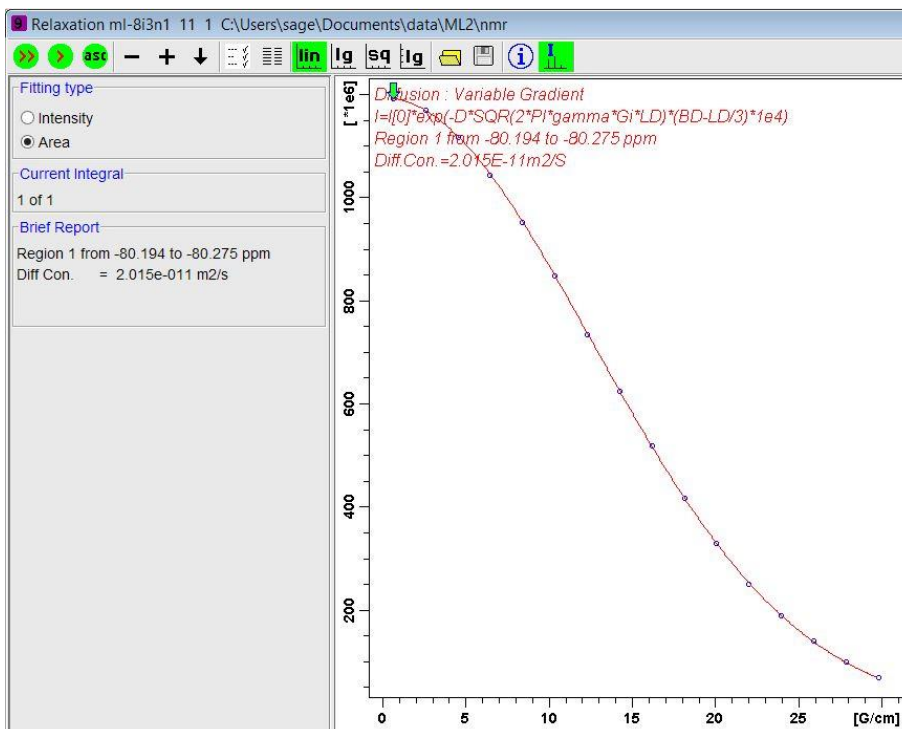


Figure 19. Fit of ^{19}F (anion) diffusion data to Stejskal-Tanner equation for $[\text{Tz8i3n1}][\text{Tf}_2\text{N}]$.

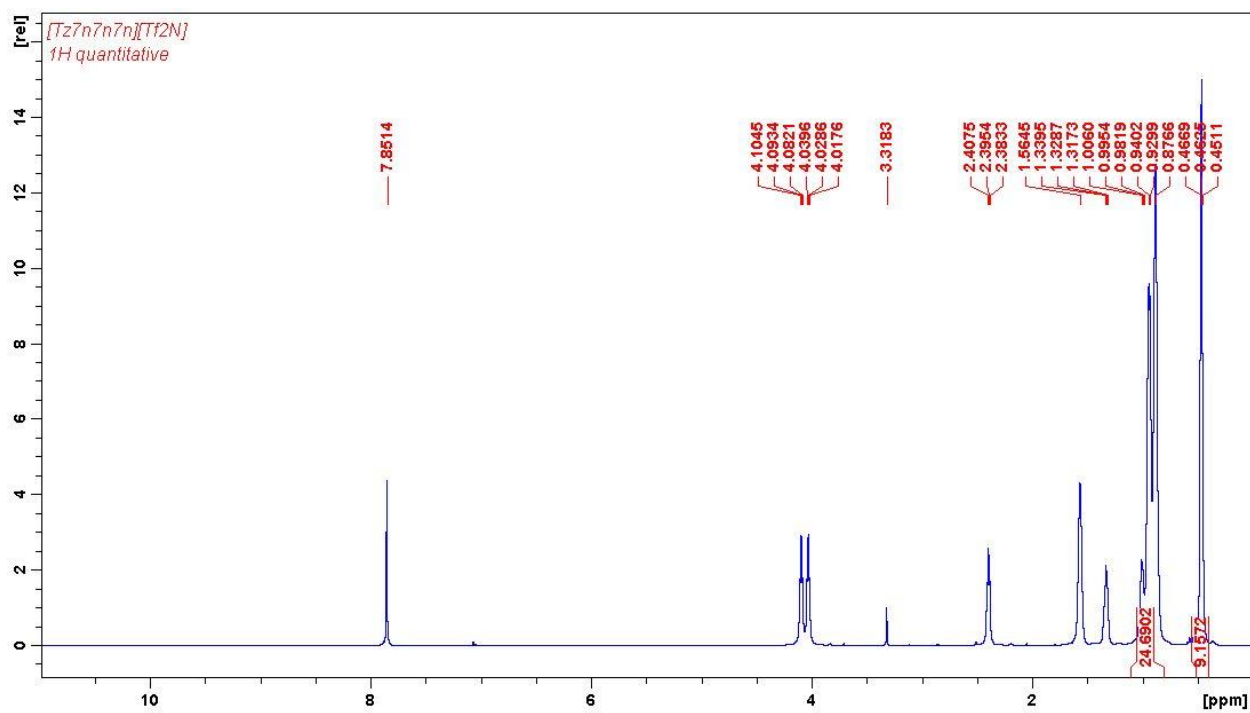


Figure 20. ¹H NMR spectrum of [Tz7n7n7n][Tf₂N].

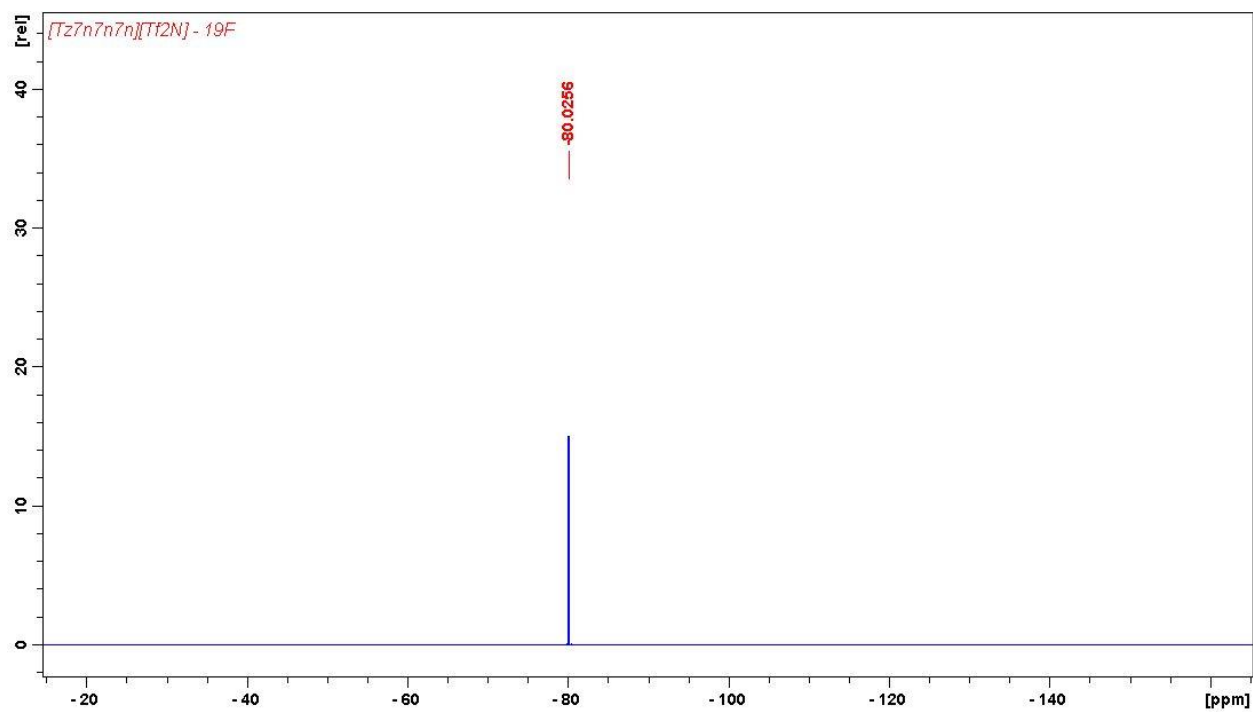


Figure 21. ¹⁹F NMR spectrum of [Tz7n7n7n][Tf₂N].

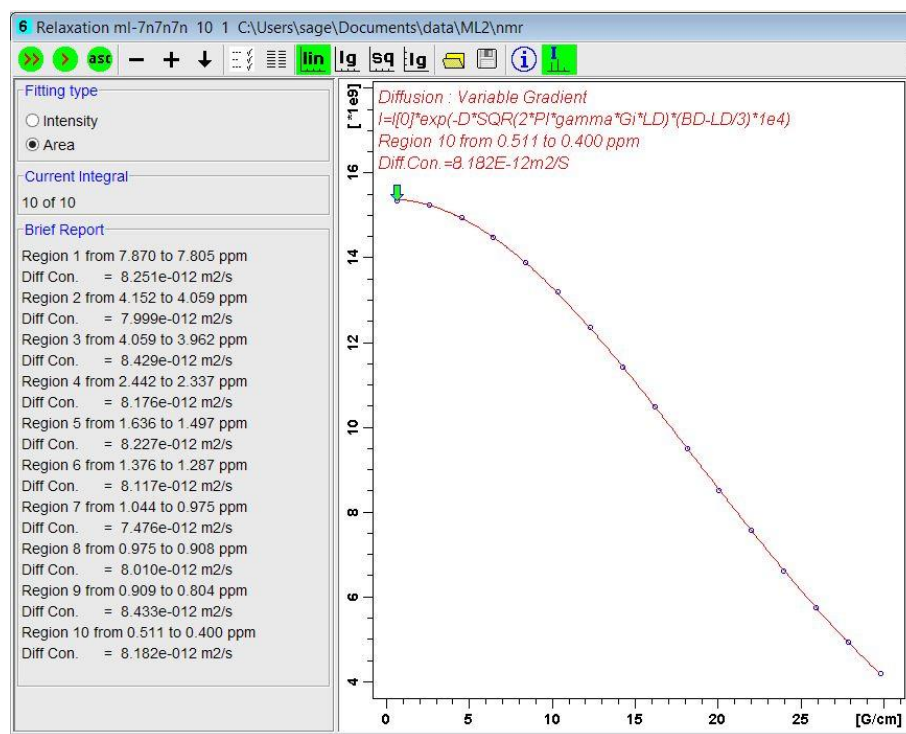


Figure 22. Fit of ^1H (cation) diffusion data to Stejskal-Tanner equation for $[\text{Tz7n7n7n}][\text{Tf}_2\text{N}]$.

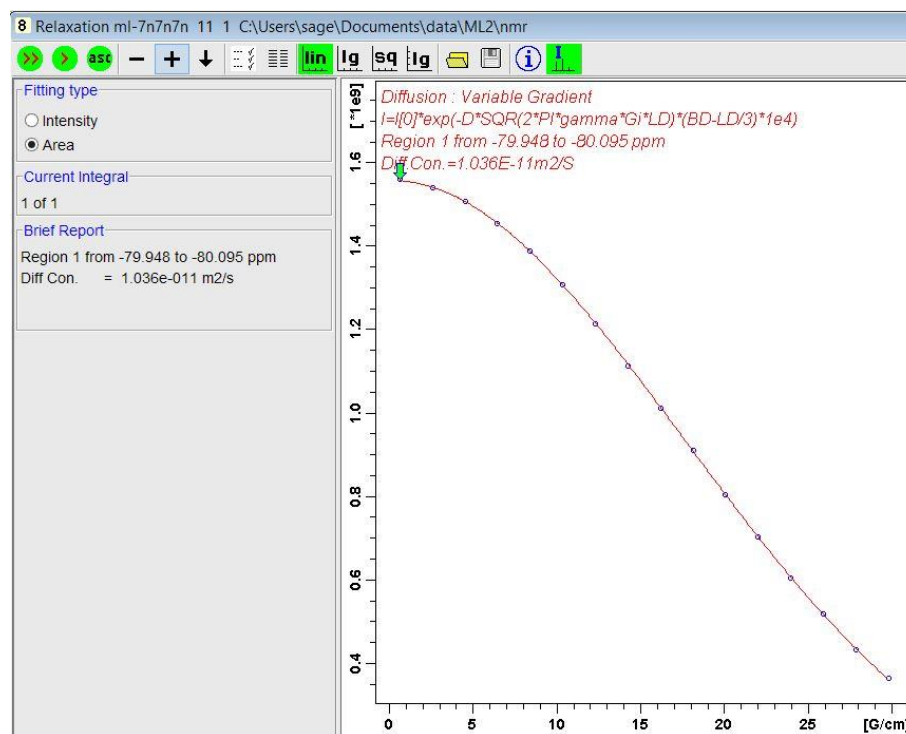


Figure 23. Fit of ^{19}F (anion) diffusion data to Stejskal-Tanner equation for $[\text{Tz7n7n7n}][\text{Tf}_2\text{N}]$.

5.5.3 ^1H and ^{19}F NMR Chemical Shift Data of Neat ILs

Table 9. NMR chemical shift data for neat $[\text{Tz3n11}][\text{Tf}_2\text{N}]$.

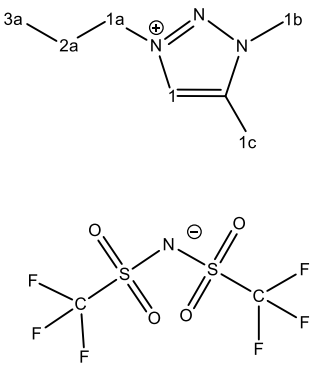
$[\text{Tz3n11}][\text{Tf}_2\text{N}]$	
	^1H Chemical Shift (ppm) <ul style="list-style-type: none"> 1 7.7070 (1H, s) 1a 3.9423 (2H, t) 2a 1.4978 (2H, sex) 3a 0.4568 (3H, t) 1b 3.6311 (3H, s) 1c 1.9643 (3H, s)
	^{19}F Chemical Shift (ppm) <ul style="list-style-type: none"> -CF₃ -80.6365 (s)

Table 10. NMR chemical shift data for neat $[\text{Tz4n11}][\text{Tf}_2\text{N}]$.

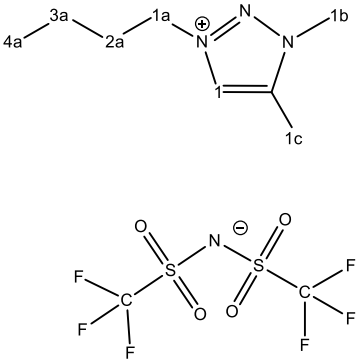
$[\text{Tz4n11}][\text{Tf}_2\text{N}]$	
	^1H Chemical Shift (ppm) <ul style="list-style-type: none"> 1 7.7319 (1H, s) 1a 3.9922 (2H, t) 2a 1.4689 (2H, quin) 3a 0.8946 (2H, sex) 4a 0.4482 (3H, t) 1b 3.6431 (3H, s) 1c 1.9774 (3H, s)
	^{19}F Chemical Shift (ppm) <ul style="list-style-type: none"> -CF₃ -80.5792 (s)

Table 11. NMR chemical shift data for neat [Tz3n3n3n][Tf₂N].

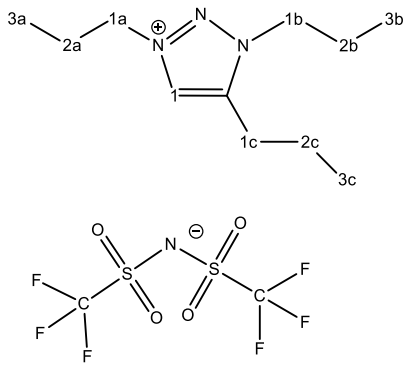
[Tz3n3n3n] [Tf₂N]		
	¹ H Chemical Shift (ppm)	
	1	7.7589 (1H, s)
	1a	4.0032 (2H, t)
	2a	1.5325 (4H, m)
	3a	0.5323 (3H, t)
	1b	3.9365 (3H, t)
	2b	1.5325 (4H, m)
	3b	0.4919 (3H, t)
	1c	2.3272 (3H, s)
	2c	1.2948 (2H, sex)
3c	0.4623 (3H, t)	
	¹⁹ F Chemical Shift (ppm)	
-CF ₃	-80.4784 (s)	

Table 12. NMR chemical shift data for neat [Tz3n3n3i][Tf₂N].

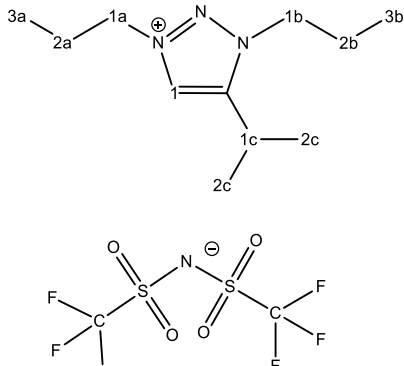
[Tz3n3n3i] [Tf₂N]		
	¹ H Chemical Shift (ppm)	
	1	7.7849 (1H, s)
	1a	4.0014 (2H, t)
	2a	1.5564 (2H, sex)
	3a	0.5015 (3H, t)
	1b	3.9582 (2H, t)
	2b	1.5331 (2H, sex)
	3b	0.4631 (3H, t)
	1c	2.7810 (1H, sep)
	2c	0.8545 (6H, d)
	¹⁹ F Chemical Shift (ppm)	
-CF ₃	-80.3859 (s)	

Table 13. NMR chemical shift data for neat [Tz3i3i3i][Tf₂N].

[Tz3i3i3i] [Tf₂N]		
	¹ H Chemical Shift (ppm)	
	1	7.7215 (1H, s)
	1a	4.5180 (1H, sep)
	2a	1.1462 (6H, d)
	1b	4.4583 (1H, sep)
	2b	1.1250 (6H, d)
	1c	2.7935 (1H, sep)
	2c	0.8660 (6H, d)
	¹⁹ F Chemical Shift (ppm)	
	-CF ₃	-80.1701 (s)

Table 14. NMR chemical shift data for neat [Tz4n14n][Tf₂N].

[Tz4n14n] [Tf₂N]		
	¹ H Chemical Shift (ppm)	
	1	7.7481 (1H, s)
	1a	4.0091 (2H, t)
	2a	1.4793 (2H, quin)
	3a	0.9675 (2H, sex)
	4a	0.4692 (6H, m)
	1b	3.6524 (3H, s)
	1c	2.3270 (3H, s)
	2c	1.2449 (2H, quin)
	3c	0.9032 (2H, sex)
4c	0.4621 (6H, m)	
	¹⁹ F Chemical Shift (ppm)	
	-CF ₃	-80.4507 (s)

Table 15. NMR chemical shift data for neat [Tz5n5n1][Tf₂N].

[Tz5n5n1] [Tf₂N]		
	¹ H Chemical Shift (ppm)	
	1	7.7745 (1H, s)
	1a	4.0279 (2H, t)
	2a	1.5314 (4H, bm)
	3a	0.95-0.84 (8H, bm)
	4a	0.95-0.84 (8H, bm)
	5a	0.4227 (6H, bm)
	1b	3.9835 (3H, t)
	2b	1.5314 (4H, bm)
	3b	0.95-0.84 (8H, bm)
	4b	0.95-0.84 (8H, bm)
	5b	0.4227 (6H, bm)
	1c	2.0167 (3H, s)
¹⁹ F Chemical Shift (ppm)		
-CF ₃	-80.3392 (s)	

Table 16. NMR chemical shift data for neat [Tz4n4n4n][Tf₂N].

[Tz4n4n4n] [Tf₂N]		
	¹ H Chemical Shift (ppm)	
	1	7.7819 (1H, s)
	1a	4.0578 (2H, t)
	2a	1.5089 (4H, quin)
	3a	1.02-0.88 (6H, m)
	4a	0.4866 (9H, m)
	1b	3.9907 (3H, t)
	2b	1.5089 (4H, quin)
	3b	1.02-0.88 (6H, m)
	4b	0.4866 (9H, m)
	1c	2.3653 (3H, t)
	2c	1.2746 (2H, quin)
	3c	1.02-0.88 (6H, m)
4c	0.4866 (9H, m)	
¹⁹ F Chemical Shift (ppm)		
-CF ₃	-80.3042 (s)	

Table 17. NMR chemical shift data for neat [Tz4i4i4i][Tf₂N].

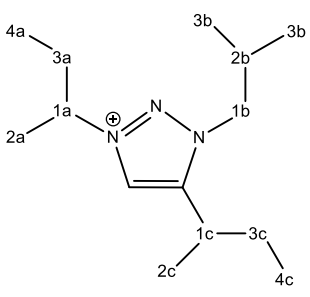
[Tz4i4i4i] [Tf₂N]		
	¹ H Chemical Shift (ppm)	
	1	8.0640 (1H, b)
	1a	4.3448 (1H, q)
	2a	1.143 (3H, d)
	3a	1.2990 (1H, m); 1.233 (1H, sex)
	4a	0.346 (3H, t)
	1b	3.8745 (2H, d)
	2b	1.887 (1H, m)
	3b	0.4856 (6H, d)
	1c	2.625 (1H, q)
	2c	0.836 (3H, d)
	3c	1.65-1.4 (2H, m)
	4c	0.4003 (3H, t)
	-CF ₃	¹⁹ F Chemical Shift (ppm)
	-80.1349 (s)	

Table 18. NMR chemical shift data for neat [Tz8i3n1][Tf₂N].

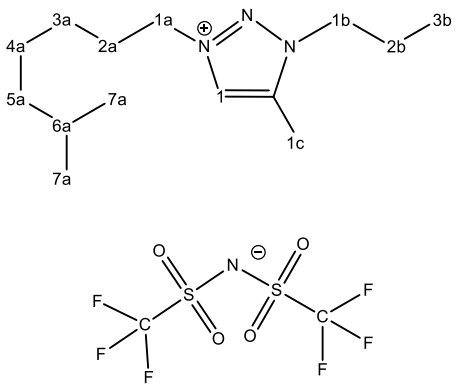
[Tz8i3n1] [Tf₂N]		
	¹ H Chemical Shift (ppm)	
	1	7.7883 (1H, s)
	1a	4.0338 (2H, t)
	2a	1.6-1.5 (4H, bm)
	3a	0.95-0.85 (4H, b)
	4a	0.95-0.85 (4H, b)
	5a	0.7314 (2H, q)
	6a	1.0666 (1H, sep)
	7a	0.4033 (1H, d)
	1b	3.9576 (2H, t)
	2b	1.6-1.5 (4H, bm)
	3b	0.5217 (3H, t)
	1c	2.0205 (3H, s)
	-CF ₃	¹⁹ F Chemical Shift (ppm)
	-80.2269 (s)	

Table 19. NMR chemical shift data for neat [Tz5n5n5n][Tf₂N].

[Tz5n5n5n] [Tf ₂ N]		
	¹ H Chemical Shift (ppm)	
	1	7.8089 (1H, s)
	1a	4.0695 (2H, t)
	2a	1.5447 (4H, quin)
	3a	1.0-0.85 (12H, bm)
	4a	1.0-0.85 (12H, bm)
	5a	0.4455 (9H, m)
	1b	4.0034 (2H, t)
	2b	1.5447 (4H, quin)
	3b	1.0-0.85 (12H, bm)
	4b	1.0-0.85 (12H, bm)
	5b	0.4455 (9H, m)
	1c	2.3748 (2H, t)
	2c	1.3089 (2H, quin)
3c	1.0-0.85 (12H, bm)	
4c	1.0-0.85 (12H, bm)	
5c	0.4455 (9H, m)	
¹⁹ F Chemical Shift (ppm)		
-CF ₃	-80.1728 (s)	

Table 20. NMR chemical shift data for neat [Tz7i7n1][Tf₂N].

[Tz7i7n1n] [Tf ₂ N]		
	¹ H Chemical Shift (ppm)	
	1	7.8193 (1H, s)
	1a	4.0725 (2H, m)
	2a	1.5644 (1H, m); 1.3584(1H, m)
	3a	0.4992 (3H, d)
	4a	0.95-0.75 (12H, bm)
	5a	1.0565 (1H, m); 0.7436 (1H, m)
	6a	0.95-0.75 (12H, bm)
	7a	0.4382 (3H, t)
	1b	3.9921 (2H, t)
	2b	1.5255 (2H, q)
	3b	0.95-0.75 (12H, bm)
	4b	0.95-0.75 (12H, bm)
	5b	0.95-0.75 (12H, bm)
6b	0.95-0.75 (12H, bm)	
7b	0.4348 (3H, t)	
1c	2.0207 (3H, s)	
¹⁹ F Chemical Shift (ppm)		
-CF ₃	-80.1654 (s)	

Table 21. NMR chemical shift data for neat [Tz7n7n3n][Tf₂N].

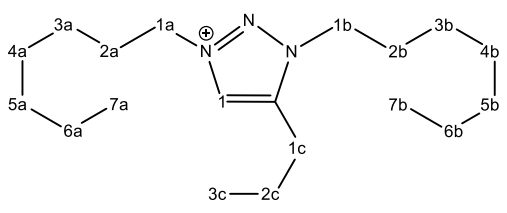
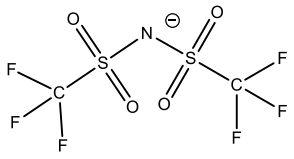
[Tz7n7n3n] [Tf₂N]	
	<p style="text-align: center;">1H Chemical Shift (ppm)</p> <p>1 7.8309 (1H, s)</p> <p>1a 4.0905 (2H, t)</p> <p>2a 1.5661 (4H, b)</p> <p>3a 0.99-0.91 (8H, b)</p> <p>4a 0.99-0.91 (8H, b)</p> <p>5a 0.91-0.84 (8H, b)</p> <p>6a 0.91-0.84 (8H, b)</p> <p>7a 0.4560 (6H, m)</p> <p>1b 4.0274 (2H, t)</p> <p>2b 1.5661 (4H, b)</p> <p>3b 0.99-0.91 (8H, b)</p> <p>4b 0.99-0.91 (8H, b)</p> <p>5b 0.91-0.84 (8H, b)</p> <p>6b 0.91-0.84 (8H, b)</p> <p>7b 0.4560 (6H, m)</p> <p>1c 2.3816 (2H, t)</p> <p>2c 1.3571 (2H, sex)</p> <p>3c 0.5989 (3H, t)</p>
	<p style="text-align: center;">¹⁹F Chemical Shift (ppm)</p> <p>-CF₃ -80.1701(s)</p>

Table 22. NMR chemical shift data for neat [Tz8i8n1][Tf₂N].

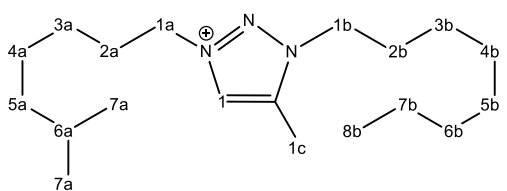
[Tz8i8n1] [Tf₂N]		
	¹ H Chemical Shift (ppm)	
	1	7.8049 (1H, s)
	1a	4.0498 (2H, t)
	2a	1.547 (4H, bm)
	3a	1.0-0.8 (14H, b)
	4a	1.0-0.8 (14H, b)
	5a	1.0-0.8 (14H, b)
	6a	1.101 (1H, m)
	7a	0.4416 (6H, d)
	1b	4.0080 (2H, t)
	2b	1.547 (4H, bm)
	3b	1.0-0.8 (14H, b)
	4b	1.0-0.8 (14H, b)
	5b	1.0-0.8 (14H, b)
	6b	1.0-0.8 (14H, b)
7b	0.7620 (2H, m)	
8b	0.4575 (3H, t)	
1c	2.0387 (3H, s)	
	¹⁹ F Chemical Shift (ppm)	
-CF ₃	-80.0996 (s)	

Table 23. NMR chemical shift data for neat [Tz7n7n7n][Tf₂N].

[Tz7n7n7n] [Tf₂N]		
	¹ H Chemical Shift (ppm)	
	1	7.8514 (1H, s)
	1a	4.0934 (2H, t)
	2a	1.5645 (4H, bm)
	3a	1.10-0.80 (24H, bm)
	4a	1.10-0.80 (24H, bm)
	5a	1.10-0.80 (24H, bm)
	6a	1.10-0.80 (24H, bm)
	7a	0.4625 (9H, bm)
	1b	4.0286 (2H, t)
	2b	1.5645 (4H, bm)
	3b	1.10-0.80 (24H, bm)
	4b	1.10-0.80 (24H, bm)
	5b	1.10-0.80 (24H, bm)
6b	1.10-0.80 (24H, bm)	
7b	0.4625 (9H, bm)	
1c	2.3654 (2H, t)	
2c	1.3287 (2H, bm)	
3c	1.10-0.80 (24H, bm)	
4c	1.10-0.80 (24H, bm)	
5c	1.10-0.80 (24H, bm)	
6c	1.10-0.80 (24H, bm)	
7c	0.4625 (9H, bm)	
¹⁹ F Chemical Shift (ppm)		
-CF ₃	-80.0256	

5.6 ELECTRICAL IMPEDANCE SPECTROSCOPY

Electrical impedance spectroscopy was performed using a Solartron SI1260 Potentiostat in conjunction with a Solartron 1252A Impedance Analyzer (Solartron Analytical, Hampshire, UK), controlled by Z-Plot (Scribner Associates, Southern Pines, NC, USA). The conductivity cell was InLab 751 (Mettler-Toledo, Columbus, OH, USA) was a dip-type conductivity cell model having platinized platinum electrodes and a rated cell constant of 0.97 cm^{-1} . The cell constant was calibrated using a $5000 \mu\text{s}$ KCl conductivity standard (Ricca Chemicals, Arlington, TX USA).

Since the frequency limitations of the impedance analyzer did not allow for visualization of any of the data points of the loop corresponding to the bulk solution, an additional circuit consisting of a 1 kOhm resistor in series with a 100uF capacitor was connected in series to the conductivity cell. The additional loop produced in the spectrum was used to verify the proper functioning of the instrument during each acquisition, as well as to create more isolation between the Faraday impedance curve, which can be affected by even small changes to the coating of the electrodes. Spectra were acquired with and without the “dummy circuit” to ensure that for both the KCl standard and several ILs to ensure that the presence of the cell did not change the measured resistance.

Conductivity measurements were carried out inside a home-built dry box. IL samples were loaded into test tubes, which were inserted into a custom-machined aluminum block heater. Temperature was controlled at $30 \text{ }^{\circ}\text{C} \pm 0.1 \text{ }^{\circ}\text{C}$, the heater unit having previously been calibrated using a K-type thermocouple in conjunction with Fluke 9150 Calibration Well.

100 data points were acquired for each measurement using a logarithmic frequency list between 10Hz and 300000Hz. DC polarization was set to zero vs. the open circuit potential. The

AC potential amplitude set to 10, 20, or 30mV, the larger values being used for the more resistive ILs. Data were plotted as a Nyquist plot using the Z-View software package (Scribner Associates). The DC resistance of the liquid was taken as the first minimum of Z'' . At least three repeat measurements were made for each IL.

APPENDIX A: COMPLETE PARAMETERS OF LINEAR REGRESSION ANALYSES

Regression Analysis: KH (23 C) [bar] versus Molar volume [cm³/mol]

The regression equation is

$$\text{KH (23 C) [bar]} = 43.0 - 0.0408 \text{ Molar volume [cm}^3\text{/mol]}$$

Predictor	Coef	SE Coef	T	P
Constant	43.009	2.062	20.86	0.000
Molar volume [cm ³ /mol]	-0.040771	0.005063	-8.05	0.000

S = 1.41597 R-Sq = 83.3% R-Sq(adj) = 82.0%

Analysis of Variance

Source	DF	SS	MS	F	P
Regression	1	130.03	130.03	64.85	0.000
Residual Error	13	26.06	2.00		
Total	14	156.09			

Unusual Observations

Obs	Molar volume [cm ³ /mol]	KH (23 C) [bar]	Fit	SE Fit	Residual	St Resid
5	354	32.200	28.574	0.436	3.626	2.69R

R denotes an observation with a large standardized residual.

Regression Analysis: KH (23 C) [bar] versus Ionicity

The regression equation is

$$\text{KH (23 C) [bar]} = 11.8 + 30.5 \text{ Ionicity}$$

Predictor	Coef	SE Coef	T	P
Constant	11.828	2.451	4.83	0.000
Ionicity	30.497	4.950	6.16	0.000

S = 1.75031 R-Sq = 74.5% R-Sq(adj) = 72.5%

Analysis of Variance

Source	DF	SS	MS	F	P
--------	----	----	----	---	---

Regression	1	116.27	116.27	37.95	0.000
Residual Error	13	39.83	3.06		
Total	14	156.09			

Unusual Observations

Obs	Ionicity	KH (23 C) [bar]	Fit	SE Fit	Residual	St Resid
9	0.631	27.800	31.087	0.848	-3.287	-2.15R

R denotes an observation with a large standardized residual.

Regression Analysis: KH (23 C) [bar] versus Excess Molar Vol

The regression equation is

KH (23 C) [bar] = 42.9 - 0.128 Excess Molar Vol

Predictor	Coef	SE Coef	T	P
Constant	42.933	2.158	19.90	0.000
Excess Molar Vol	-0.12808	0.01672	-7.66	0.000

S = 1.47585 R-Sq = 81.9% R-Sq(adj) = 80.5%

Analysis of Variance

Source	DF	SS	MS	F	P
Regression	1	127.78	127.78	58.66	0.000
Residual Error	13	28.32	2.18		
Total	14	156.09			

Unusual Observations

Obs	Excess Molar Vol	KH (23 C) [bar]	Fit	SE Fit	Residual	St Resid
5	110	32.200	28.896	0.479	3.304	2.37R
15	181	21.000	19.766	0.978	1.234	1.12 X

R denotes an observation with a large standardized residual.

X denotes an observation whose X value gives it large leverage.

Regression Analysis: KH (23 C) [bar] versus Molar volume [cm, Ionicity

The regression equation is

KH (23 C) [bar] = 32.0 - 0.0281 Molar volume [cm³/mol] + 12.2 Ionicity

Predictor	Coef	SE Coef	T	P
Constant	31.987	6.156	5.20	0.000
Molar volume [cm ³ /mol]	-0.028065	0.008190	-3.43	0.005
Ionicity	12.186	6.479	1.88	0.084

S = 1.29518 R-Sq = 87.1% R-Sq(adj) = 85.0%

Analysis of Variance

Source	DF	SS	MS	F	P
Regression	2	135.964	67.982	40.53	0.000
Residual Error	12	20.130	1.677		
Total	14	156.093			

Source	DF	Seq SS
Molar volume [cm3/mol]	1	130.029
Ionicity	1	5.935

Unusual Observations

Obs	Molar volume [cm3/mol]	KH (23 C) [bar]	Fit	SE Fit	Residual	St Resid
5	354	32.200	29.235	0.531	2.965	2.51R
9	404	27.800	28.337	1.019	-0.537	-0.67 X

R denotes an observation with a large standardized residual.
 X denotes an observation whose X value gives it large leverage.

Regression Analysis: KH (23 C) [bar] versus Excess Molar Vol, Ionicity

The regression equation is
 KH (23 C) [bar] = 30.3 - 0.0836 Excess Molar Vol + 14.3 Ionicity

Predictor	Coef	SE Coef	T	P
Constant	30.325	5.171	5.86	0.000
Excess Molar Vol	-0.08362	0.02205	-3.79	0.003
Ionicity	14.310	5.503	2.60	0.023

S = 1.22855 R-Sq = 88.4% R-Sq(adj) = 86.5%

Analysis of Variance

Source	DF	SS	MS	F	P
Regression	2	137.981	68.991	45.71	0.000
Residual Error	12	18.112	1.509		
Total	14	156.093			

Source	DF	Seq SS
Excess Molar Vol	1	127.777
Ionicity	1	10.204

Unusual Observations

Obs	Excess Molar Vol	KH (23 C) [bar]	Fit	SE Fit	Residual	St Resid
5	110	32.200	29.597	0.482	2.603	2.30R

R denotes an observation with a large standardized residual.

Regression Analysis: Ionicity versus Excess Molar Vol

The regression equation is

Ionicity = 0.881 - 0.00311 Excess Molar Vol

Predictor	Coef	SE Coef	T	P
Constant	0.88108	0.09051	9.73	0.000
Excess Molar Vol	-0.0031065	0.0007015	-4.43	0.001

S = 0.0619135 R-Sq = 60.1% R-Sq(adj) = 57.1%

Analysis of Variance

Source	DF	SS	MS	F	P
Regression	1	0.075174	0.075174	19.61	0.001
Residual Error	13	0.049833	0.003833		
Total	14	0.125007			

Unusual Observations

Obs	Excess Molar Vol	Ionicity	Fit	SE Fit	Residual	St Resid
9	122	0.6315	0.5016	0.0163	0.1299	2.17R
15	181	0.3179	0.3192	0.0410	-0.0013	-0.03 X

R denotes an observation with a large standardized residual.

X denotes an observation whose X value gives it large leverage.

BIBLIOGRAPHY

- (1) Wilkes, J. S.: A short history of ionic liquids-from molten salts to neoteric solvents. *Green Chem.* **2002**, *4*, 73-80.
- (2) Gordon, C. M.; Muldoon, M. J.; Wagner, M.; Hilgers, C.; Davis, J. H.; Wasserscheid, P.: Synthesis and Purification. In *Ionic Liquids in Synthesis*; Wiley-VCH Verlag GmbH & Co. KGaA, 2008; pp 7-55.
- (3) Russina, O.; Triolo, A.: New experimental evidence supporting the mesoscopic segregation model in room temperature ionic liquids. *Faraday Discuss.* **2012**, *154*, 97-109.
- (4) Matsumoto, H.: Electrochemical Windows of Room-Temperature Ionic Liquids (RTILs). In *Electrochemical Aspects of Ionic Liquids*; John Wiley & Sons, Inc., 2011; pp 43-63.
- (5) Plechkova, N. V.; Seddon, K. R.: Ionic liquids: "designer" solvents for green chemistry. John Wiley & Sons, Inc., 2007; pp 105-130.
- (6) Seddon, K. R.: Ionic liquids: A taste of the future. *Nat. Mater.* **2003**, *2*, 363-365.
- (7) Predel, T.; Schlücker, E.; Wasserscheid, P.; Gerhard, D.; Arlt, W.: Ionic Liquids as Operating Fluids in High Pressure Applications. *Chemical Eng. Technol.* **2007**, *30*, 1475-1480.
- (8) Wang, H.; Gurau, G.; Rogers, R. D.: Ionic liquid processing of cellulose. *Chem. Soc. Rev.* **2012**, *41*, 1519-1537.
- (9) Vancov, T.; Alston, A.-S.; Brown, T.; McIntosh, S.: Use of ionic liquids in converting lignocellulosic material to biofuels. *Renew. Energ.* **2012**, *45*, 1-6.
- (10) Vagt, U.: Cellulose dissolution and processing with ionic liquids. Wiley-VCH Verlag GmbH & Co. KGaA, 2010; Vol. 6; pp 123-136.
- (11) Pinkert, A.; Marsh, K. N.; Pang, S.; Staiger, M. P.: Ionic liquids and their interaction with cellulose. *Chem. Rev.* **2009**, *109*, 6712-6728.
- (12) Zhang, X.; Zhang, X.; Dong, H.; Zhao, Z.; Zhang, S.; Huang, Y.: Carbon capture with ionic liquids: overview and progress. *Energy Environ. Sci.* **2012**, *5*, 6668-6681.
- (13) Yu, C.-H.; Huang, C.-H.; Tan, C.-S.: A review of CO₂ capture by absorption and adsorption. *Aerosol Air Qual. Res.* **2012**, *12*, 745-769.
- (14) Yang, Z.-Z.; Zhao, Y.-N.; He, L.-N.: Carbon dioxide chemistry: task-specific ionic liquids for carbon dioxide capture/activation and subsequent conversion. *RSC Adv.* **2011**, *1*, 545-567.
- (15) Ramdin, M.; de, L. T. W.; Vlugt, T. J. H.: State-of-the-Art of CO₂ Capture with Ionic Liquids. *Ind. Eng. Chem. Res.* **2012**, *51*, 8149-8177.
- (16) Lee, Z. H.; Lee, K. T.; Bhatia, S.; Mohamed, A. R.: Post-combustion carbon dioxide capture: Evolution towards utilization of nanomaterials. *Renew. Sust. Energ. Rev.* **2012**, *16*, 2599-2609.

- (17) Karadas, F.; Atilhan, M.; Aparicio, S.: Review on the Use of Ionic Liquids (ILs) as Alternative Fluids for CO₂ Capture and Natural Gas Sweetening. *Energy Fuels* **2010**, *24*, 5817-5828.
- (18) Takao, K.; Bell, T. J.; Ikeda, Y.: Actinide Chemistry in Ionic Liquids. *Inorg.Chem.* **2012**, *52*, 3459-3472.
- (19) Plechkova, N. V.; Seddon, K. R.: Applications of ionic liquids in the chemical industry. *Chem. Soc. Rev.* **2008**, *37*, 123-150.
- (20) Urahata, S. M.; Ribeiro, M. C. C.: Structure of ionic liquids of 1-alkyl-3-methylimidazolium cations: A systematic computer simulation study. *J. Chem. Phys.* **2004**, *120*, 1855-1863.
- (21) Del, P. M. G.; Voth, G. A.: On the Structure and Dynamics of Ionic Liquids. *J. Phys. Chem. B* **2004**, *108*, 1744-1752.
- (22) Wang, Y.; Voth, G. A.: Unique Spatial Heterogeneity in Ionic Liquids. *J. Am. Chem. Soc.* **2005**, *127*, 12192-12193.
- (23) Wang, Y.; Voth, G. A.: Tail Aggregation and Domain Diffusion in Ionic Liquids. *J. Phys. Chem. B* **2006**, *110*, 18601-18608.
- (24) Canongia Lopes, J. N.; Costa Gomes, M. F.; Pádua, A. A. H.: Nonpolar, Polar, and Associating Solutes in Ionic Liquids. *J. Phys. Chem. B* **2006**, *110*, 16816-16818.
- (25) Canongia Lopes, J. N. A.; Pádua, A. A. H.: Nanostructural Organization in Ionic Liquids. *J. Phys. Chem. B* **2006**, *110*, 3330-3335.
- (26) Triolo, A.; Russina, O.; Bleif, H.-J.; Di, C. E.: Nanoscale Segregation in Room Temperature Ionic Liquids. *J. Phys. Chem. B* **2007**, *111*, 4641-4644.
- (27) Triolo, A.; Russina, O.; Fazio, B.; Triolo, R.; Di, C. E.: Morphology of 1-alkyl-3-methylimidazolium hexafluorophosphate room temperature ionic liquids. *Chem. Phys. Lett.* **2008**, *457*, 362-365.
- (28) Xiao, D.; Hines, L. G., Jr.; Li, S.; Bartsch, R. A.; Quitevis, E. L.; Russina, O.; Triolo, A.: Effect of Cation Symmetry and Alkyl Chain Length on the Structure and Intermolecular Dynamics of 1,3-Dialkylimidazolium Bis(trifluoromethanesulfonyl)amide Ionic Liquids. *J. Phys. Chem. B* **2009**, *113*, 6426-6433.
- (29) Macchiagodena, M.; Gontrani, L.; Ramondo, F.; Triolo, A.; Caminiti, R.: Liquid structure of 1-alkyl-3-methylimidazolium-hexafluorophosphates by wide angle x-ray and neutron scattering and molecular dynamics. *J. Chem. Phys.* **2011**, *134*, 114521/1-114521/15.
- (30) Hardacre, C.; Holbrey, J. D.; Mullan, C. L.; Youngs, T. G. A.; Bowron, D. T.: Small angle neutron scattering from 1-alkyl-3-methylimidazolium hexafluorophosphate ionic liquids ([C_nmim][PF₆], n = 4, 6, and 8). *J. Chem. Phys.* **2010**, *133*, 074510-7.
- (31) Russina, O.; Gontrani, L.; Fazio, B.; Lombardo, D.; Triolo, A.; Caminiti, R.: Selected chemical-physical properties and structural heterogeneities in 1-ethyl-3-methylimidazolium alkyl sulfate room temperature ionic liquids. *Chem. Phys. Lett.* **2010**, *493*, 259-262.
- (32) Bradley, A. E.; Hardacre, C.; Holbrey, J. D.; Johnston, S.; McMath, S. E. J.; Nieuwenhuyzen, M.: Small-Angle X-ray Scattering Studies of Liquid Crystalline 1-Alkyl-3-methylimidazolium Salts. *Chem. Mater.* **2002**, *14*, 629-635.
- (33) Martinelli, A.; Marechal, M.; Ostlund, A.; Cambedouzou, J.: Insights into the interplay between molecular structure and diffusional motion in 1-alkyl-3-methylimidazolium ionic liquids: a combined PFG NMR and X-ray scattering study. *Phys. Chem. Chem. Phys.* **2013**, *15*, 5510-5517.

- (34) Mizuhata, M.; Maekawa, M.; Deki, S.: Ordered structure in room temperature molten salts containing aliphatic quaternary ammonium ions. *ECS Trans.* **2007**, *3*, 89-95.
- (35) Triolo, A.; Russina, O.; Fazio, B.; Appetecchi, G. B.; Carewska, M.; Passerini, S.: Nanoscale organization in piperidinium-based room temperature ionic liquids. *J. Chem. Phys.* **2009**, *130*, 164521-6.
- (36) Baltus, R. E.; Counce, R. M.; Culbertson, B. H.; Luo, H.; DePaoli, D. W.; Dai, S.; Duckworth, D. C.: Examination of the potential of ionic liquids for gas separations. *Sep. Sci. Technol.* **2005**, *40*, 525-541.
- (37) Blath, J.; Christ, M.; Deubler, N.; Hirth, T.; Schiestel, T.: Gas solubilities in room temperature ionic liquids - Correlation between RTiL-molar mass and Henry's law constant. *Chem. Eng. J.* **2011**, *172*, 167-176.
- (38) Hu, Y.-F.; Liu, Z.-C.; Xu, C.-M.; Zhang, X.-M.: The molecular characteristics dominating the solubility of gases in ionic liquids. *Chem. Soc. Rev.* **2011**, *40*, 3802-3823.
- (39) Anthony, J. L.; Anderson, J. L.; Maginn, E. J.; Brennecke, J. F.: Anion Effects on Gas Solubility in Ionic Liquids. *J. Phys. Chem. B* **2005**, *109*, 6366-6374.
- (40) Anderson, J. L.; Dixon, J. K.; Brennecke, J. F.: Solubility of CO₂, CH₄, C₂H₆, C₂H₄, O₂, and N₂ in 1-Hexyl-3-methylpyridinium Bis(trifluoromethylsulfonyl)imide: Comparison to Other Ionic Liquids. *Acc. Chem. Res.* **2007**, *40*, 1208-1216.
- (41) Price, W. S.: NMR Studies of Translational Motion: Principles and Application. **2009**, 1-57.
- (42) Borucka, A. Z.; Bockris, J. O. M.; Kitchener, J. A.: Test of the Applicability of the Nernst-Einstein Equation to Self-Diffusion and Conduction of Ions in Molten Sodium Chloride. *J. Chem. Phys.* **1956**, *24*, 1282-1282.
- (43) Bockris, J. O. M.; Hooper, G. W.: Self-diffusion in molten alkali halides. *Discuss. Faraday Soc.* **1961**, *32*, 218-236.
- (44) Majumdar, D. K.: Transport properties in molten electrolytes. *Z. Phys. Chem.* **1966**, *233*, 377-87.
- (45) Angell, C. A.; Tomlinson, J. W.: Self-diffusion and electrical conductance measurements on solutions of cadmium in molten cadmium chloride. *Discuss. Faraday Soc.* **1961**, *32*, 237-249.
- (46) Price, W. S.: Pulsed-field gradient nuclear magnetic resonance as a tool for studying translational diffusion: Part 1. Basic theory. *Concept. Magnet. Res.* **1997**, *9*, 299-336.
- (47) Stejskal, E. O.; Tanner, J. E.: Spin Diffusion Measurements: Spin Echoes in the Presence of a Time-Dependent Field Gradient. *J. of Chem. Phys.* **1965**, *42*, 288-292.
- (48) Sinnaeve, D.: The Stejskal-Tanner equation generalized for any gradient shape—an overview of most pulse sequences measuring free diffusion. *Concept. Mag. Res. A* **2012**, *40A*, 39-65.
- (49) Robinson, R. A.; Stokes, R. H.: *Electrolyte solutions, the measurement and interpretation of conductance, chemical potential, and diffusion in solutions of simple electrolytes*; 2d, rev. ed.; Butterworths, London, 1965.
- (50) Diard, J. P.; Landaud, P.; Gorrec, B.; Montella, C.: Automatic measurement of the conductivity of an electrolyte solution by FFT electrochemical impedance spectroscopy. *J. Appl. Electrochem.* **1992**, *22*, 1180-1184.
- (51) Barral, G.; Diard, J. P.; Gorrec, B.; Tri, L.; Montella, C.: Impédances de cellules de conductivité. I. Détermination des plages de fréquence de mesure de la conductivité. *J. Appl. Electrochem.* **1985**, *15*, 913-924.

- (52) Macdonald, J. R.: Binary electrolyte small-signal frequency response. *J. of Electroanal. Chem. Interfacial Electrochem.* **1974**, *53*, 1-55.
- (53) Every, H. A.; Bishop, A. G.; MacFarlane, D. R.; Oradd, G.; Forsyth, M.: Transport properties in a family of dialkylimidazolium ionic liquids. *Phys. Chem. Chem. Phys.* **2004**, *6*, 1758-1765.
- (54) Hatano, N.; Watanabe, M.; Takekiyo, T.; Abe, H.; Yoshimura, Y.: Anomalous Conformational Change in 1-Butyl-3-methylimidazolium Tetrafluoroborate-D₂O Mixtures. *J. Phys. Chem. A* **2012**, *116*, 1208-1212.
- (55) Tokuda, H.; Hayamizu, K.; Ishii, K.; Susan, M. A. B. H.; Watanabe, M.: Physicochemical Properties and Structures of Room Temperature Ionic Liquids. 1. Variation of Anionic Species. *J. Phys. Chem. B* **2004**, *108*, 16593-16600.
- (56) Tokuda, H.; Hayamizu, K.; Ishii, K.; Susan, M. A. B. H.; Watanabe, M.: Physicochemical Properties and Structures of Room Temperature Ionic Liquids. 2. Variation of Alkyl Chain Length in Imidazolium Cation. *J. Phys. Chem. B* **2005**, *109*, 6103-6110.
- (57) Tokuda, H.; Ishii, K.; Susan, M. A. B. H.; Tsuzuki, S.; Hayamizu, K.; Watanabe, M.: Physicochemical Properties and Structures of Room-Temperature Ionic Liquids. 3. Variation of Cationic Structures. *J. Phys. Chem. B* **2006**, *110*, 2833-2839.
- (58) Tokuda, H.; Tsuzuki, S.; Susan, M. A. B. H.; Hayamizu, K.; Watanabe, M.: How Ionic Are Room-Temperature Ionic Liquids? An Indicator of the Physicochemical Properties. *J. Phys. Chem. B* **2006**, *110*, 19593-19600.
- (59) Tokuda, H.; Tsuzuki, S.; Susan, M. A. B. H.; Hayamizu, K.; Watanabe, M.: How Ionic Are Room-Temperature Ionic Liquids? An Indicator of the Physicochemical Properties. *J. Phys. Chem. B* **2006**, *110*, 19593-19600.
- (60) Sangoro, J.; Iacob, C.; Serghei, A.; Naumov, S.; Galvosas, P.; Karger, J.; Wespe, C.; Bordusa, F.; Stoppa, A.; Hunger, J.; Buchner, R.; Kremer, F.: Electrical conductivity and translational diffusion in the 1-butyl-3-methylimidazolium tetrafluoroborate ionic liquid. *J. Chem. Phys.* **2008**, *128*, 214509.
- (61) Nulwala, H. B.; Tang, C. N.; Kail, B. W.; Damodaran, K.; Kaur, P.; Wickramanayake, S.; Shi, W.; Luebke, D. R.: Probing the structure-property relationship of regioisomeric ionic liquids with click chemistry. *Green Chem.* **2011**, *13*, 3345-3349.
- (62) Allen, J. J.; Schneider, Y.; Kail, B. W.; Luebke, D. R.; Nulwala, H.; Damodaran, K.: Nuclear Spin Relaxation and Molecular Interactions of a Novel Triazolium-Based Ionic Liquid. *J. Phys. Chem. B* **2013**, *117*, 3877-3883.
- (63) Thompson, R. L.; Damodaran, K.; Luebke, D.; Nulwala, H.: Aprotic Heterocyclic Anion Triazolide Ionic Liquids - A New Class of Ionic Liquid Anion Accessed by the Huisgen Cycloaddition Reaction. *Synlett.* **2013**, *24*, 1093-1096.
- (64) Kumelan, J.; Perez-Salado, K. A.; Tuma, D.; Maurer, G.: Solubility of CO₂ in the Ionic Liquids [bmim][CH₃SO₄] and [bmim][PF₆]. *J. Chem. Eng. Data* **2006**, *51*, 1802-1807.
- (65) Ohta, S.; Shimizu, A.; Imai, Y.; Abe, H.; Hatano, N.; Yoshimura, Y.: Peculiar concentration dependence of H/D exchange reaction in 1-butyl-3-methylimidazolium tetrafluoroborate-D₂O mixtures. *Open J. Phys. Chem.* **2011**, *1*, 70-76.
- (66) Hollóczki, O.; Terleczyk, P.; Szieberth, D.; Mourgas, G.; Gudat, D.; Nyulászi, L.: Hydrolysis of Imidazole-2-ylidenes. *J. Am. Chem. Soc.* **2010**, *133*, 780-789.
- (67) Zheng, W.; Mohammed, A.; Hines, L. G.; Xiao, D.; Martinez, O. J.; Bartsch, R. A.; Simon, S. L.; Russina, O.; Triolo, A.; Quitevis, E. L.: Effect of Cation Symmetry on the

Morphology and Physicochemical Properties of Imidazolium Ionic Liquids. *J. Phys. Chem. B* **2011**, *115*, 6572-6584.

(68) Appetecchi, G. B.; Montanino, M.; Zane, D.; Carewska, M.; Alessandrini, F.; Passerini, S.: Effect of the alkyl group on the synthesis and the electrochemical properties of N-alkyl-N-methyl-pyrrolidinium bis(trifluoromethanesulfonyl)imide ionic liquids. *Electrochim. Acta* **2009**, *54*, 1325-1332.

(69) Edward, J. T.: Molecular volumes and the Stokes-Einstein equation. *J. Chem. Ed.* **1970**, *47*, 261.

(70) MacFarlane, D. R.; Forsyth, M.; Izgorodina, E. I.; Abbott, A. P.; Annat, G.; Fraser, K.: On the concept of ionicity in ionic liquids. *Phys. Chem. Chem. Phys.* **2009**, *11*, 4962-4967.

(71) Angell, C. A.; Byrne, N.; Belieres, J.-P.: Parallel Developments in Aprotic and Protic Ionic Liquids: Physical Chemistry and Applications. *Acc. Chem. Res.* **2007**, *40*, 1228-1236.

(72) Hunt, P. A.: Why Does a Reduction in Hydrogen Bonding Lead to an Increase in Viscosity for the 1-Butyl-2,3-dimethyl-imidazolium-Based Ionic Liquids?†. *J. Phys. Chem. B* **2007**, *111*, 4844-4853.

(73) Bowser, S. University of Pittsburgh. Unpublished results. 2012.

(74) Tanaka, S.; Sugihara, Y.; Sakamoto, A.; Ishii, A.; Nakayama, J.: The Thiosulfinyl Group Serves as a Stereogenic Center and Shows Diamagnetic Anisotropy Similar to That of the Sulfinyl Group. *J. Am. Chem. Soc.* **2003**, *125*, 9024-9025.

(75) Jin, H.; O'Hare, B.; Dong, J.; Arzhantsev, S.; Baker, G. A.; Wishart, J. F.; Benesi, A. J.; Maroncelli, M.: Physical Properties of Ionic Liquids Consisting of the 1-Butyl-3-Methylimidazolium Cation with Various Anions and the Bis(trifluoromethylsulfonyl)imide Anion with Various Cations. *J. Phys. Chem. B* **2007**, *112*, 81-92.